

CH₄ Parameter Estimation in CLM4.5bgc Using Surrogate Global Optimization

J. Müller¹, R. Paudel², C.A. Shoemaker³, J. Woodbury³, Y. Wang³, and
N. Mahowald²

¹Center for Computational Sciences and Engineering, Lawrence Berkeley National Laboratory,
Berkeley, CA, 94720

²Earth and Atmospheric Sciences, Cornell University, Ithaca, NY, 14853

³School of Civil and Environmental Engineering, Cornell University, Ithaca, NY, 14853

Correspondence to: J. Müller (juliane.mueller2901@gmail.com)

Abstract. Over the anthropocene methane has increased dramatically. Wetlands are one of the major sources of methane to the atmosphere, but the role of changes in wetland emissions is not well understood. The Community Land Model (CLM) of the Community Earth System Models contains a module to estimate methane emissions from natural wetlands and rice paddies. Our comparison
5 of CH₄ emission observations at 16 sites around the planet reveals, however, that there are large discrepancies between the CLM predictions and the observations. The goal of our study is to adjust the model parameters in order to minimize the root mean squared error (RMSE) between model predictions and observations. These parameters have been selected based on a sensitivity analysis. Because of the cost associated with running the CLM simulation (15 to 30 minutes on the Yellow-
10 stone Supercomputing Facility), only relatively few simulations can be allowed in order to find a near-optimal solution within an acceptable time. Our results indicate that the parameter estimation problem has multiple local minima. Hence, we use a computationally efficient global optimization algorithm that uses a radial basis function (RBF) surrogate model to approximate the objective function. We use the information from the RBF to select parameter values that are most promising with
15 respect to improving the objective function value. We show with pseudo data that our optimization algorithm is able to make excellent progress with respect to decreasing the RMSE. Using the true CH₄ emission observations for optimizing the parameters, we are able to significantly reduce the overall RMSE between observations and model predictions by about 50%. The CLM predictions with the optimized parameters agree for northern and tropical latitudes more with the observed data
20 than when using the default parameters and the emission predictions are higher than with default settings in northern latitudes and lower than default settings in the tropics.

1 Introduction and Motivation

Methane is the second most important greenhouse gas in terms of radiative forcing (Myhre et al., 2013) and thus a major concern regarding climate change. Natural wetlands as well as human activities such as agriculture (for example, rice cultivation) contribute to the methane emissions (Ciais et al., 2013). The role of wetlands in the total budget of methane, as well as in driving inter-annual variability and changes in the methane growth rate is not well understood (e.g. Bloom et al. (2010); Dlugokencky et al. (2011)). The Community Land Model (CLM), which is the land component of the Community Earth System Model (CESM), is equipped with a methane module that models methane emissions (Meng et al., 2012; Riley et al., 2011). There are several parameters in CLM related to the methane emission computations. The methane emissions estimated by the model are sensitive to the exact parameter values although these parameters are not well known (e.g. Meng et al. (2012); Riley et al. (2011); Wania et al. (2010)). Riley et al. (2011) and Meng et al. (2012) reported significant differences in model simulations and observations in both site-level methane emissions and the global budget. One important source of uncertainty is associated with the parametrization since the methane module has numerous parameters and they are yet to be identified empirically due to the lack of field data (Riley et al., 2011). In this study our goal is to use surrogate model optimization techniques in order to adjust the methane-related parameters of the CLM such that the differences between the simulated and observed methane emissions at 16 sites around the globe are minimized.

40

For computing an objective function value, we have to do a computationally expensive simulation with CLM4.5bgc in order to obtain the methane emission predictions at each observation site. CLM4.5bgc and related codes are deterministic models, i.e., the simulated CH_4 emissions for a given parameter set will always be the same whenever we run the model for the same parameter set. In an optimization framework where the goal is to find the best set of parameters to minimize the objective function, one obstacle is the computation time that is needed to obtain a single objective function value. Only a few hundred function evaluations can be allowed in order to obtain a solution within reasonable time. Moreover, the objective function value must be computed by running a simulation model, and thus an analytic description of the objective function is not available (black-box). Therefore, gradient information, which is important for many optimization algorithms, is not available. Due to the black-box nature of the objective function, it is also not known whether or not the objective function is convex and has only one local minimum (which corresponds to the global minimum) or if there are several local and global minima in the objective function landscape.

55 These characteristics of the objective function (computationally expensive, black-box, possibly multi-modal) do not allow the application of a gradient-based optimization algorithm because, on the one hand, the derivatives would have to be computed numerically (which may be inaccurate and requires many expensive function evaluations), and, on the other hand, gradient-based algorithms

generally stop at a local minimum if the initial guess is not close to the global minimum.

60

For calibrating the parameters of other CLM modules, Markov Chain Monte Carlo (MCMC) methods and Kalman filters have been used in the literature (Lo et al., 2010; Prihodko et al., 2008; Schuh et al., 2010; Solonen et al., 2012; Sun et al., 2013; Tian et al., 2008; Turner et al., 2009; Zeng et al., 2013). MCMC, however, requires generally thousands of function evaluations (Ray and Swiler, 65 2014) and is thus not applicable for obtaining solutions in an acceptable time for computationally expensive problems. When using Ensemble Kalman Filters, assumptions about the underlying parameter distributions must be made and generally a large number of observations is necessary for the method to be effective. Furthermore, evolutionary strategies such as simulated annealing, particle swarm, and differential evolution methods have been used for parameter tuning in the climate 70 area (Yang et al., 2012, 2013). However, these methods generally require many function evaluations in order to obtain good solutions.

Other methods that have recently gained interest for parameter tuning are based on data assimilation (see, for example, Han et al. (2014); Moore et al. (2008)). In order to produce good parameter 75 estimates, these methods require in general many observations. In our optimization problem, however, the number of observations at each site is very low (between 10 and 79 observations distributed over one to three years), and thus data assimilation techniques are not suitable because of the low number of observations. Ray and Swiler (2014) use a computationally cheap surrogate for CLM on which MCMC is used to reduce the number of costly simulations required during the optimization. 80 In contrast to Ray and Swiler (2014), we apply an adaptive surrogate model during the optimization. Instead of relying on a surrogate that is based only on a limited number of initial sample points, we iteratively improve our surrogate by incorporating new data (new objective function values) that become available during the optimization.

85 We use surrogate model based global optimization algorithms because they have been shown to find near-optimal solutions within few hundred function evaluations for computationally expensive multimodal black-box problems (Aleman et al., 2009; Giunta et al., 1997; Regis, 2011; Simpson et al., 2001). Surrogate models are used as computationally cheap approximations of the objective function. During the optimization, information from the surrogate model is used to carefully select a 90 new promising point in the variable domain at which the computationally expensive objective function will be evaluated. The surrogate model is updated throughout the optimization whenever new data are obtained.

Several surrogate model algorithms have been developed in the literature that use different surrogate 95 model types. The efficient global optimization algorithm by Jones et al. (1998), for example,

uses a kriging surrogate model and selects a new sample point by maximizing an expected improvement function. Gutmann (2001) uses radial basis function (RBF) surrogate models to approximate the expensive objective function and a new sample point is selected by minimizing a so-called bumpiness measure. Regis and Shoemaker (2007, 2013) also use RBF models and new function evaluation points are selected by a stochastic method. Müller and Piché (2011) developed a framework for automatically computing ensembles of various surrogate model types and Müller and Shoemaker (2014) extended the study to investigate the influence of different sampling strategies on the solution quality. Here for the first time, we apply a state-of-the-art RBF surrogate optimization algorithm to the problem of land surface emissions of methane and describe the results. As far as we know, no other groups have applied optimization techniques to find better parameters for methane emission models, and thus our work represents an innovative approach to an important land-atmosphere interaction.

The remainder of this paper is organized as follows. In Section 2 we briefly describe the CLM and the configuration we used for predicting the methane emissions and we give information about the individual observation sites. We also provide the mathematical description of the optimization problem. In Section 3 we summarize the methane-related parameters in CLM4.5bgc and show the results of a sensitivity analysis with which we determined the parameters that are most important for the optimization. We describe the surrogate optimization approach for solving the problem in Section 4. Section 5 contains information about the setup of our numerical experiments and we discuss the results of the optimization. We draw conclusions in Section 6. The appendix contains additional information about the methane equations and the observation sites.

2 Model Description, Configuration, and Mathematical Problem Description

2.1 Model Description

We used the Community Land Model Version 4.5 (CLM4.5), a land component of the Community Earth System Model (CESM) (Hurrell et al., 2013) which contains a detailed biophysics, hydrology, and biogeochemistry representation (Koven et al., 2013; Oleson et al., 2013). CLM4.5 is fully prognostic with respect to the carbon and nitrogen state variables in the vegetation, litter, and soil organic matter, as well as methane emissions (Koven et al., 2013; Thornton et al., 2007, 2009) and it is the most updated version of the model available.

We selected the latest version of CLM with improved biogeochemistry (CLM4.5bgc) over CLM4.0-CN. The major improvements in CLM4.5bgc include the incorporation of vertically-resolved soil carbon dynamics, an alternate decomposition cascade from the Century soil model, and a more detailed representation of nitrification and denitrification based on the Century nitrogen model (Koven et al., 2013). The hydrology of CLM4.5 has been improved to better represent the hydraulic proper-

ties of frozen soils, perched water tables, snow cover fraction, and lakes (Subin et al., 2012; Swenson and Lawrence, 2012; Swenson et al., 2012).

In previous versions, simulation of ecosystem productivity was too low in high latitudes and perhaps too high in low latitudes (Thornton et al., 2007, 2009). However, CLM4.5bgc has substantially increased the productivity in high latitudes, which may be overpredicted (Koven et al., 2013).

We used a mechanistic methane emission model, which is a module integrated in CLM4.5bgc (Meng et al., 2012; Riley et al., 2011). The model simulates the physical and biogeochemical processes regulating terrestrial methane fluxes such as methane production, methane oxidation, methane and oxygen transport through aerenchyma of wetland plants, ebullition, and methane and oxygen diffusion through soil (Riley et al., 2011). Meng et al. (2012) added constraints on methane emissions such as the effects of redox potential and soil pH to improve the predictions of methane emissions as well as the ability to simulate satellite derived inundation fraction (Prigent et al., 2007; Ringeval et al., 2010).

The model has been compared to the limited site-level observations of methane emissions (many of the sites have very sparse spatial and temporal data coverage, and directly measured climate forcing was unavailable at any of the sites) (Meng et al., 2012; Riley et al., 2011). Additionally, the model was compared with the results from three recent global atmospheric inversion estimates of methane emissions (Riley et al., 2011). In these comparisons, simulated emissions agreed relatively well with the observed emissions at some of the sites. However, there are considerable differences in seasonality and magnitude at other sites. The simulated patterns and magnitudes of annual-average methane emissions are consistent with the results from atmospheric inversion across most latitude bands. The limitations are discussed in Riley et al. (2011).

2.2 Model Configuration and Data

Although the land model can be used interactively within CESM, we use it at specific points driven by appropriate meteorology (Oleson et al., 2013). At each site, we forced the model with NCEP/NCAR's reanalysis atmospheric forcing data sets (Qian et al., 2006). These data sets include precipitation, temperature, wind speeds, and solar radiation. We also forced the model with transient atmospheric carbon dioxide concentrations, aerosol deposition data, and nitrogen deposition data that is available in CLM4.5. Please note that this model is a deterministic model, and thus will give the same answer every time it is simulated when driven by observationally-based datasets as done here.

In this study we used a total of six natural wetland sites and ten rice paddy sites (see Tables B1 and B2 in Appendix B). We chose the wetland sites from varying geographical regions such as the tropics, mid-latitudes, and high-latitudes to account for the zonal variability. We selected the rice paddy sites such as to cover the major rice-growing regions with a focus on Asia.

170

The water table depth is one of the critical factors for methane emissions from natural wetlands because it determines the extent of anoxic and oxic soil zones where methane is produced and oxidized, respectively (Bloom et al., 2010; Grunfeld and Brix, 1999). Methane is produced in the wetlands from litter and dead vegetation remnants in anoxic conditions. The changes in the water table position also influence the moisture conditions of the soil and therefore affect the methane emissions. Here, we prescribed the measured water table position at each wetland site (except Panama) based on previous studies. Since the measured water table depths at Panama were not available, we used modeled water table positions (similar to Walter and Heimann (2000)). For the point simulations, the methane emissions were calculated only from the saturated portion of the soil (i.e. below the water table) when the water table is below the surface. The prescribed water table depth is used in the methane model for calculating anaerobic conditions, production, and oxidation.

180

Most of these wetland sites usually have peat soils with varying depths underlain by mineral soil. We also forced each wetland site with measured pH and a specific plant functional type (PFT). The PFT reflects the phenological and physiological characteristics of the vegetation (Oleson et al., 2013). Since the wetland PFT was not available in CLM4.5, we choose PFTs that are available in CLM4.5 and that closely match the specific vegetation types of the individual sites. We use C_3 arctic grass for Salmisuo, C_3 non-arctic grass for Alberta, Michigan, and Minnesota, and C_4 grass for Florida and Panama. Other surface data required to perform the point simulation include soil color and soil texture which we extracted from the global grid data sets available in CLM4.5.

190

For the point simulations at the rice paddy sites we only considered the rice growing season. The flooding and drainage dates are shown in Table C1 in Appendix C. We assumed that the fields were submerged during the simulation period between initial flooding and final drainage. A common feature of these sites during the growing season is that the water was not drained until harvest. We prescribed the C_3 crop PFT for all rice paddy sites, and assumed an optimal pH for the methane production whenever the pH value was not available. The dominant soil types at these sites are loam and clay. Other soil-related information such as soil color and texture are derived from the global grid datasets.

200

To bring the terrestrial carbon and nitrogen cycles close to steady-state conditions, we spun up both wetland and rice paddy sites for 1850 conditions (atmospheric CO_2 concentrations, nitrogen

deposition, aerosol deposition, and land use) driven by a repeating 25-year subset (1948-1972) of the meteorological forcing data for more than 2000 years. Then, we performed transient simulations
 205 from 1850 to the simulation starting year of each site to generate the initial conditions file.

Additionally, we conducted global simulations of methane emissions from natural wetlands for 1993-2004. For these simulations, the grid cell averaged methane emissions were considered which accounts for methane emissions from both the inundated and non-inundated portion of the grid
 210 cell. Since the CLM4.5 simulated saturated fraction (an index of inundation) was substantially greater than the estimates from satellite observations and did not match the spatio-temporal pattern of variability (Riley et al., 2011), we prescribed the model with inundation fraction derived from multi-satellite observations for 1993-2004 (Prigent et al., 2007). Similar to point simulations, the global simulations were forced with NCEP/NCAR reanalysis atmospheric forcing data from 1948
 215 to 2004 (Qian et al., 2006). The simulations were also spun up to steady-state conditions driven by atmospheric CO₂, nitrogen deposition, aerosol deposition, and land use in the year 1850 and a repeated 25-year (1948-1972) subset of the meteorological forcing.

2.3 Mathematical Problem Formulation

The goal of our study is to improve the methane emission predictions of CLM4.5bgc by tuning the
 220 methane-related parameters such that the model better fits the observations. We use the CH₄ emission observation data for the locations and observation periods shown in Tables B1 and B2. Given the observation data at the $M = 16$ locations, the goal is to minimize the root mean squared errors (RMSEs) between the CLM4.5bgc methane emission predictions and the observations at each site simultaneously. In order to tackle the problem, we formulate it such that we minimize the weighted
 225 sum of the RMSEs as follows:

$$\min f(\mathbf{x}) = \sum_{i=1}^M w_i r_i(\mathbf{x}) \quad (1a)$$

$$\text{s.t. } -\infty < x_k^l \leq x_k \leq x_k^u < \infty, \quad k = 1, \dots, d, \quad (1b)$$

where d denotes the problem dimension (the number of optimization parameters), and x_k^l and x_k^u are
 230 the lower and upper bounds of variable x_k , respectively. The RMSE

$$r_i(\mathbf{x}) = \sqrt{\frac{1}{N_i} \sum_{j=1}^{N_i} [O_{i,j} - S_{i,j}(\mathbf{x})]^2}, \quad i = 1, \dots, M, \quad (2)$$

is computed for each location i . N_i is the number of observations available at location i , $O_{i,j}$ denotes the j th methane emission observation at location i , and $S_{i,j}$ denotes the corresponding methane emission predicted by CLM4.5bgc. The weights w_i are computed based on the means of the CH₄

235 emissions at the observation locations as follows. Denote

$$a_i = \frac{1}{N_i} \sum_{j=1}^{N_i} O_{i,j} \quad (3)$$

the mean CH₄ emission at location i , $i = 1, \dots, M$. The weight w_i for the i th location is then defined by

$$w_i = \frac{g_i}{\sum_{i=1}^M g_i}, \quad (4)$$

240 where

$$g_i = \frac{\max_{i=1, \dots, M} a_i}{a_i}, \quad (5)$$

where it is assumed that $a_i > 0$ for all i . The goal is to give each location approximately equal influence in the weighted sum of RMSEs, i.e., we assign locations with large mean CH₄ values small weights such that these locations have approximately the same influence on the weighted sum as lo-
245 cations with low emissions. Otherwise, locations with large emissions would dominate the sum (1a) because their RMSEs would accordingly be larger. In that case the optimization would be driven by minimizing the RMSE of the site(s) with the largest emissions. There are also other methods of how w_i could be determined. In the numerical experiments, we will investigate also the possibilities of assigning equal weights to each observation site and assigning weights derived from grouping the
250 observation sites into zones. Another possibility would be to apply clustering algorithms in order to determine groups of observation sites with similar characteristics. For this possibility, however, different clustering methods and different numbers of desired clusters will lead to different groups and different weight adjustments. Lastly, the problem could be formulated as multi-objective optimization problem, for example, with 16 objectives and the goal of minimizing each observation site's
255 RMSE individually, or as bi-objective optimization problem by minimizing the sum of the weighted RMSE values of northern and southern locations at the same time. However, each objective function evaluation is very expensive, and thus the number of evaluations that can be done to obtain the Pareto front in a multi-objective setting is limited. Our focus is on demonstrating that single objective global optimization analysis is useful in identifying reasonable parameter values.

260 3 Methane-Related Parameters in CLM4.5bgc and Sensitivity Analysis

CLM4.5bgc has 21 parameters related to the methane emission predictions. The parameter names, their upper and lower bounds, and default values are shown in Table 1. The upper and lower bounds have been derived based on reported values in the literature (see Table C1 in Appendix C). How these parameters are used in the model is detailed in Riley et al. (2011) and Meng et al. (2012) and
265 we repeat the important equations in Appendix A. The default parameter values v_k are available in

the CLM4.5bgc (see Table 1).

270 Optimization problems become increasingly more complex and difficult to solve as the number of parameters increases (curse of dimensionality). Thus, we determine first which of these 21 parameters are the most sensitive and thus the most important for the optimization. By sensitive we refer to parameters that when changed slightly lead to a significant change in emission predictions. Insensitive parameters, on the other hand, can be changed and do not (or comparatively only very mildly) change the emission predictions and can thus be excluded from the optimization, which decreases the problem dimension.

275

We conducted analyses for each observation site in which we investigated to which of these 21 parameters the methane emission predictions of CLM4.5bgc are the most sensitive. We altered the value of each parameter $k = 1, \dots, d$ by, respectively, adding and subtracting 20% of the variable range and we recorded the absolute change in emission predictions, i.e. we ran CLM4.5bgc with 280 perturbed parameter values

$$(a) \ x_k = \min\{v_k + 0.2(x_k^u - x_k^l), x_k^u\}, \forall k = 1, \dots, d \text{ when increasing } v_k \text{ for 20\%, and}$$

$$(b) \ x_k = \max\{v_k - 0.2(x_k^u - x_k^l), x_k^l\}, \forall k = 1, \dots, d \text{ when decreasing } v_k \text{ for 20\%}$$

for each parameter separately.

285 There are several parameters that are relatively important to the sensitivity test for all 16 observation sites, but there are also parameters that are important for some locations and less important for others. Tables 2 and 3 show the sensitive and insensitive parameters together with the number of locations (out of 16) for which these parameters are important and unimportant, respectively. Thus, in the optimization we consider only the parameters in Table 2 since these parameters are 290 the most important at most locations. Please note that, due to (nonlinear) relationships between the parameters, for many parameters the effects of individual parameters will be opposite but act in a similar manner, indicating that some parameters may be difficult to optimize for. In order to limit the number of parameters we consider, while allowing for the largest range in behavior, we combine information from the sensitivity study with information about the methane flux equations themselves 295 (described in more detail in Appendix A). The most important parameters from the sensitivity study come from the dominant three terms in the methane flux equation, which are production (parameters 1, 2, and 21), oxidation (parameters 7, 8, 9, and 10), and aerenchyma transport (parameters 13, 15, 16, and 17). The first four parameters chosen are also the most important parameters at all 16 sites (see Table 2). Because production is the most important term, there are two parameters from 300 production that the sensitivity studies indicate are the most important, namely one that controls globally the methane production flux (F_{CH4} , parameter 2), and one term that controls the temperature

dependency of the methane production (Q10CH4, parameter 1). Another parameter that influences methane at all the sites comes from the oxidation equation (VMAX_CH4_OXID, parameter 7), and the final parameter that is important at all 16 sites is the parameter controlling the aerenchyma transport (SCALE_FACTOR_AERE, parameter 13). The above four parameters are the most sensitive parameters, and thus are easy to choose, as well as cover most of the important processes we want to investigate. For the last parameter, we include one parameter that controls how inundation affects methane production (MINO2LIM, parameter 21). Inundation is an important process for controlling methane flux, since there is an order of magnitude more methane coming from wet areas than dry, and thus having one parameter which changes the model’s sensitivity to inundation is appropriate.

4 Surrogate Models and Surrogate Model Algorithms

4.1 Surrogate Models

Surrogate models are used in optimization algorithms that aim to solve computationally expensive black-box problems. Surrogate models serve as computationally cheap approximations of the expensive simulation model (Booker et al., 1999), i.e., $f(\mathbf{x}) = s(\mathbf{x}) + e(\mathbf{x})$, where $f(\cdot)$ denotes the true expensive objective function, $s(\cdot)$ denotes the computationally inexpensive surrogate model, and $e(\cdot)$ denotes the difference between both. Surrogate models are used throughout the optimization to guide the search for promising solutions. The computationally expensive objective function is evaluated only at few selected points, and thus it is possible to find near-optimal solutions with only very few expensive function evaluations.

There are different surrogate model types such as radial basis functions (RBFs) (Gutmann, 2001; Müller et al., 2013; Powell, 1992; Regis and Shoemaker, 2007, 2009; Wild and Shoemaker, 2013), kriging (Davis and Ierapetritou, 2009; Forrester et al., 2008; Jones et al., 1998; Simpson et al., 2001), polynomial regression models (Myers and Montgomery, 1995), and multivariate adaptive regression splines (Friedman, 1991). There are also mixture models (also known as ensemble models) that exploit information from several different surrogate model types (Goel et al., 2007; Müller and Piché, 2011; Müller and Shoemaker, 2014; Viana et al., 2009). In general any type of surrogate model may be used in a surrogate model optimization algorithm. In this study, we use RBFs because they have been shown to perform better in comparison to other surrogate model types (Müller and Shoemaker, 2014).

An RBF interpolant is defined as follows:

$$s(\mathbf{x}) = \sum_{\iota=1}^n \lambda_{\iota} \phi(\|\mathbf{x} - \mathbf{x}_{\iota}\|) + p(\mathbf{x}), \quad (6)$$

335 where $\phi(\tau) = \tau^3$ denotes the cubic radial basis function whose corresponding polynomial tail is linear ($p(\mathbf{x}) = b_0 + \mathbf{b}^T \mathbf{x}$), and $\mathbf{x}_\ell, \ell = 1, \dots, n$, denotes the points at which the objective function has already been evaluated. The parameters $\lambda_\ell \in \mathbb{R}, \ell = 1, \dots, n$, and the parameters $b_0 \in \mathbb{R}$ and $\mathbf{b} = [b_1, \dots, b_d] \in \mathbb{R}^d$ are determined by solving the following linear system of equations

$$\begin{bmatrix} \Phi & \mathbf{P} \\ \mathbf{P}^T & \mathbf{0} \end{bmatrix} \begin{bmatrix} \boldsymbol{\lambda} \\ \mathbf{c} \end{bmatrix} = \begin{bmatrix} \mathbf{F} \\ \mathbf{0} \end{bmatrix}, \quad (7)$$

340 where $\Phi_{\ell\nu} = \phi(\|\mathbf{x}_\ell - \mathbf{x}_\nu\|), \ell, \nu = 1, \dots, n$, $\mathbf{0}$ is a matrix with all entries 0 of appropriate dimension, and

$$\mathbf{P} = \begin{bmatrix} \mathbf{x}_1^T & 1 \\ \mathbf{x}_2^T & 1 \\ \vdots & \vdots \\ \mathbf{x}_n^T & 1 \end{bmatrix}, \quad \boldsymbol{\lambda} = \begin{bmatrix} \lambda_1 \\ \lambda_2 \\ \vdots \\ \lambda_n \end{bmatrix}, \quad \mathbf{c} = \begin{bmatrix} b_1 \\ b_2 \\ \vdots \\ b_d \\ b_0 \end{bmatrix}, \quad \mathbf{F} = \begin{bmatrix} f(\mathbf{x}_1) \\ f(\mathbf{x}_2) \\ \vdots \\ f(\mathbf{x}_n) \end{bmatrix}. \quad (8)$$

The matrix in (7) is invertible if and only if $\text{rank}(\mathbf{P}) = d + 1$ (Powell, 1992).

4.2 Surrogate Global Optimization Algorithm

345 Surrogate global optimization algorithms follow in general the steps shown in Algorithm 1.

Algorithm 1 General Surrogate Global Optimization Algorithm

- 1: Select points from the variable domain to create an initial experimental design.
 - 2: Do the expensive objective function evaluations (here the CLM4.5bgc simulations) at the points selected in Step 1.
 - 3: Fit the surrogate model (here the RBF model) to the data from Steps 1 and 2.
 - 4: Use the information from the surrogate model to select the new evaluation point \mathbf{x}_{new} .
 - 5: Do the expensive evaluation at $\mathbf{x}_{\text{new}}: f_{\text{new}} = f(\mathbf{x}_{\text{new}})$ (here, run CLM 4.5bgc for the parameter input vector \mathbf{x}_{new}).
 - 6: **if** Stopping criterion is not met (the maximum number of allowed function evaluations has not been reached)
then
 - 7: Update the surrogate model and go to Step 4.
 - 8: **else**
 - 9: Return the best solution found during the optimization.
 - 10: **end if**
-

We use the DYCORS algorithm by Regis and Shoemaker (2013) for the optimization of the methane-related parameters of CLM4.5bgc. The reader is referred to this publication for the details of the algorithm. Since the parameters have significantly differing ranges (see Table 1), we scale all parameters to the interval $[0, 1]$ when selecting new sample sites. When doing the computationally

350 expensive CLM4.5bgc simulations, we scale the parameters back to their original ranges. Thus, the
perturbation radius used in DYCORS is the same for each variable.

We create a symmetric Latin hypercube initial experimental design with $2(d + 1)$ points and run
CLM4.5bgc at the selected parameter vectors in order to compute the objective function values. We
355 then fit the cubic RBF model to the data and generate two sets of candidate points for the next expen-
sive function evaluation (the next CLM4.5bgc run at the 16 sites). The first set of candidate points is
generated as described by Regis and Shoemaker (2013) by randomly perturbing the best point found
so far. The second set of candidate points is generated by uniformly selecting random points from
the whole variable domain. Thus, we create twice as many candidate points as DYCORS. The goal
360 of using uniformly random points from the whole variable domain is to obtain candidates that are
far away from the best point found so far, and hence if selected as new evaluation point, the search
is more global (exploration by function evaluation at points that are far away from already sampled
points).

365 We use the same criteria as in DYCORS for determining the best candidate point (using the RBF
approximation to predict the objective function values at the candidate points, compute the distance
of the candidate points to the set of already sampled points, and compute a weighted score of these
two measures where the weights cycle through a predefined pattern). In order to guarantee that the
matrix in equation (7) is well-conditioned, we ensure (as done in Regis and Shoemaker (2013)) that
370 the sample points are sufficiently far away from previously evaluated points by discarding candi-
date points that are closer than a given threshold distance to previously evaluated points. We run
CLM4.5bgc at each of the 16 observation sites using the one newly selected sample point as input
parameter vector to obtain the corresponding objective function value. We update the RBF model
with the new data and iterate until we have reached the maximum number of allowed function eval-
375 uations.

5 Numerical Experiments

In this section we discuss the setup and results of the numerical experiments. In a first set of ex-
periments (pseudo data case), we generate synthetic (pseudo) data and treat it as if it were the real
measurement data in order to assess how well our optimization approach performs. For these ex-
380 periments we know the optimal solution. In the second set of experiments (real data case), we use
the measured methane emission data and apply the optimization algorithm. The goal in the second
set of experiments is to find a parameter set that reduces the objective function value (the weighted
RMSE in equation (1a)) from its default value (the RMSE when using CLM4.5bgc's default param-
eter settings, see also Table 1, column v_k). Finally, we run CLM4.5bgc globally with the best set of

385 parameters found during the optimization of the real data case and investigate how much the default
model predictions and the model predictions with the optimized parameter values differ from each
other.

We did experiments with $d = 5$ and $d = 11$ parameters respectively. For the $d = 5$ experiments,
390 we used parameters 1, 2, 7, 13, and 21 (Table 2). Thus, we have parameters related to three types
of CH₄ emission, namely oxidation (parameter 7), aerenchyma (parameter 13), and production (pa-
rameters 1, 2, 21). For the 11-parameter optimization, we used all variables shown in Table 2.

For each set of experiments we ran the optimization algorithm three times in order to examine the
395 influence of the random component in the algorithm (random initial experimental design and ran-
dom generation of candidate points). We allowed 800 function evaluations for the five-dimensional
problem and 1000 evaluations for the 11-dimensional problem. The question of how many function
evaluations need to be performed in order to obtain a fixed level of solution accuracy is problem
dependent. For computationally-expensive optimization problems, such as the problem we consider
400 here, the time for evaluating the objective function and the totally available time for obtaining a
solution usually defines how many evaluations can be done with any algorithm. Results for many
difficult computationally-expensive optimization problems (for example, problems with multiple lo-
cal minima) indicate that surrogate global optimization methods can usually obtain more accurate
results compared to non-surrogate methods with the same limited number of evaluations (see, for
405 example, Mugunthan et al. (2005)). It is a very difficult problem to find the best values of the param-
eters for climate models, and the more evaluations one does, in general the better the answer.

The weights w_i in equation (1a) were for the pseudo data case computed based on the pseudo
observations (see Section 5.1) at each of the 16 sites at the same dates for which we also have real
410 measurements. For the real data case, the weights were computed based on the actual measurements.
The weights are given in Table D1 in Appendix D.

Solving problem (1a) requires running CLM4.5bgc for each input vector \mathbf{x} of parameter values
and for each of the 16 observation sites. We run CLM4.5bgc on the Yellowstone Supercomputing
415 Facility (Computational and Information Systems Laboratory, 2012). Each simulation at a single
location takes between 15 and 30 minutes. We do the simulations for the 16 sites in parallel in order
to speed up the objective function evaluation time.

5.1 Pseudo Data Case

We assessed the performance of the optimization algorithm by investigating how well the algorithm
420 could find the model parameters that were used for creating the pseudo data. For this purpose, we

ran CLM4.5bgc with default parameter values $v_k, k = 1, \dots, d$, at all 16 sites for the same time span for which we also have observation data (see Tables B1 and B2 in Appendix B) and we record the model's predictions for the same dates at which the methane emissions were measured. We use this as our pseudo observation data that we want to match in the optimization, i.e., the goal of the optimization is to start from a set of parameter vectors that is different from the default parameter values and to recover the default parameter values by optimization. For the default parameter values, the objective function value will be zero, which is the global minimum of the pseudo data case.

5.1.1 Results for $d = 5$

Figure 1 shows the progress plots of the three optimization trials T1, T2, and T3. Illustrated is the development of the best objective function value found within the given number of function evaluations (horizontal axis). The fewer evaluations needed for reducing the objective function value, the better. The plot shows that the objective function value is reduced significantly in each of the three trials from a value of over 30 to about 5 within less than 150 function evaluations and close to zero towards the end of the optimization. Table 4 shows the best parameter values found during each of the three optimization trials together with the default parameter values. The table shows that the RMSE after 800 function evaluations is not exactly zero (which can be expected from an approximation method), but the default parameter values are matched closely.

5.1.2 Results for $d = 11$

Figure 2 shows the objective function value development as the number of function evaluations increases for the 11-dimensional case for the three trials T1, T2, and T3. The figure shows a rapid decrease of the objective function value from over 50 to less than 10 within 100 evaluations, which shows that the surrogate model algorithm is very efficient at finding improved solutions. Although the objective function value improvement over the following function evaluations is lower, we can see that the algorithm still makes progress and if we allowed more than 1000 evaluations, the objective function value would be further improved (which also follows from the global convergence property of the DYCORS algorithm).

Table 5 shows the parameter values of the best of the three trials (T3) together with the default parameter values and the variable vector CP that was evaluated during the optimization and that has a *worse* objective function value than the best solution, but that is *closer* to the default parameter values. This point has the same parameter values as T3 for all but two parameters, namely, parameters 10 (Q10_CH4OXID) and 21 (MINO2LIM), which we indicate by bold numbers. For these two parameters, the point CP is closer to the global optimum, but it has a worse objective function value. This indicates a multimodality of the objective function (getting closer to the true global minimum

requires an increase in the objective function value, i.e., the algorithm has to escape from a local basin of attraction). This multimodality makes the search for the global optimum significantly more difficult.

460 In order to examine the impact of the differences between default and optimized parameter values on the model prediction, we use the best parameter vector of each trial and plot the corresponding CH₄ emission predictions against the predictions when using the default parameter values in Figure 3. We can see that although we do not exactly match the default parameter values, the model's predictions when using the optimized parameters are very close to the predictions when using the
465 default parameter values (all points in the scatter plot lie close to or on the dashed line which represents agreement of default and optimized predictions). As also reflected in the best RMSE value reported in the legend, T3 matches the default data best and T2 has the largest differences.

This result indicates that the calibration problem is not "identifiable" for all parameter sets, indicating that more than one parameter set can give a very similar result in terms of the objective
470 function value. For example, for the model $y = \frac{\alpha}{\beta} \mathbf{x} + \gamma$, there are many combinations of values for α and β that lead to the same value of y as long as $\alpha = \kappa\beta$ for some constant κ . With only five parameters as described in the previous section, the parameter values obtained from the optimization did match very closely those of the default case used to create the pseudo data, and thus with this
475 small set of parameters the problem was identifiable. However, for 11 parameters, we did encounter the identifiability problem. In some disciplines such parameters are called "hidden". For example, estimating α and γ in the previous example with $y = \frac{\alpha}{\beta} \mathbf{x} + \gamma$ when β is given would be identifiable. However, estimating α , β , and γ is no longer identifiable.

480 It would be desirable to have an identifiable model, but the CLM (and probably other climate modules) have a number of interacting parameters and multiplicative nonlinearities, and thus there is no guarantee that all parameters are identifiable. This is reinforced by the data in Table 5, which indicates that the surface over which the optimization algorithm searches in the 11 parameter case is multi-modal, i.e., there are multiple local minima and it is possible for two (or more) parameter
485 sets to yield the same objective function value (here RMSE). Hence the inability of the optimization to find the exact set of parameters that was used for generating the pseudo data is a problem caused by the complexity and multiplicative nonlinearities of the CLM model, not by the choice of the optimization method. However, the optimization analysis for both pseudo data cases (with 5 and 11 parameters, respectively) shows that the chosen optimization method is able to find a set of
490 parameter values that has a low prediction error. The multi-modality in Table 5 does indicate the need for a global (not a local) optimization method.

5.2 Real Data Case

In the real data case, we use the actual methane emission measurements at each of the 16 observation sites for computing the objective function value. Since we only have very few observations for each site and no information about measurement errors, we did not exclude any of the measurements from the optimization although there might be outliers. Also for the real data case we examine the case for $d = 5$ and $d = 11$ variables.

5.2.1 Results for $d = 5$

The progress of the development of the objective function value for the three trials T1, T2, and T3, respectively, is illustrated in Figure 4 which also shows in the legend the lowest RMSE value found in each of the three trials. The RMSE was efficiently reduced from over 155 to below 115 within the first 150 function evaluations. Thereafter the objective function value improvement was at a significantly lower rate. All three trials return a solution with approximately the same objective function value.

The parameter values of the best solutions found in the three trials are shown in Table 6 where also the default parameter values are given for comparison. We can see that the three optimized solutions are approximately the same and significantly different from the default case. We can also see that three of the five optimized parameter values are on or very close to the boundary of the variable domain (shown in bold), indicating that improvements of the objective function value may be possible by increasing the parameter range. However, it is not possible due to physical constraints and at this point, we do not have information about possible wider parameter ranges than the ones we used in this study.

Figures 5 and 6 show the CH_4 emission predictions of CLM4.5bgc when using the default and the optimized parameter values for two selected observation sites (one wetland and one rice paddy site) together with the actual observation data. The legends show the associated RMSE value before applying the weights for computing (1a). We can see that the optimized solution actually worsens the predictions for Alberta (the RMSE value with default parameters is about 209 and with optimized parameters, the value is about 221, which is about 6% worse). For Central Java, on the other hand, the RMSE values of the optimized solutions are significantly better than for the default values (the default RMSE is about 221 and the optimized RMSE values are about 48, which is an improvement of over 350%). In both figures we can also see that despite the large differences between optimized and default parameter values, the trend in the predictions of CLM4.5bgc is the same, i.e., when the predicted CH_4 emissions with default parameters increase so do the predicted emissions when using the optimized parameters and vice versa.

5.2.2 Results for $d = 11$

Figure 7 shows the progress plots for each of the three trials together with the best objective function values found (legend) for the 11-dimensional case. The best objective function value found is about
530 equal for each of the three trials. The figure shows that in each trial the algorithm is able to efficiently reduce the objective function value within the first 200 function evaluations. The improvement after 200 function evaluations is significantly slower.

Table 7 shows the parameter values of the best solution found in each of the three trials and the
535 default parameter values. The table shows that for some parameters, for example, parameters 1, 7, and 8, all trials lead to approximately the same values (which are different from the default parameter values). For the remaining parameters, the values corresponding to the best solution found differ significantly for each trial and differ also from the default parameter values. Also for the 11-dimensional problem, some parameter values corresponding to the best solution found are on the
540 upper or lower boundary of the parameter range (for example, parameters 1, 8, 13, 15, indicated in bold).

Since all three solutions have approximately the same objective function values, but the points differ greatly, it is an indicator that we either have a multi-modal surface in which some minima
545 assume approximately the same objective function values, or we have a very flat valley in which many points assume similar objective function values. Both possibilities make it very difficult for gradient-based optimization algorithms to find the global optimum. In the first case, the optimization algorithm will get trapped in a local optimum if it is not started close to the global minimum. In the second case, the gradient-based algorithm would require many function evaluations because many
550 steps and gradient computations are necessary due to a very small step size. The surrogate optimization algorithm overcomes this problem.

Table 8 shows the unweighted RMSE values (before applying the weights in (1a) for computing the objective function value) between observations and simulations using the default parameters
555 (column 5), the best parameters of optimization trial T1 of the 11-dimensional case (column 4), and the best parameters of trial T2 of the 5-dimensional case, respectively. The table shows that with our optimization we were able to decrease the default RMSE for four sites in the 5-dimensional case and for six sites in the 11-dimensional case. The RMSE is lower at seven sites for the 11-dimensional case than for the 5-dimensional case. Since we minimized a weighted sum of all RMSE values, it
560 can be expected that the RMSE at some locations may be worse for the optimized case than for the default case. We can see that for two of the improved sites (Java and Cuttack), the improvement is very large, and thus the overall RMSE of the optimized solution is lower than for the default param-

eters.

565 Figures 8 and 9 show the observed CH₄ emissions, the predictions with the default parameter values, and the predictions using the optimized parameter values for Alberta (Canada) and Central Java (Indonesia). For both sites we can see that the predictions with the optimized parameters have lower RMSEs than when using the default parameter values (note that the reported RMSEs in the legend are not weighted as done in equation (1a)). For Central Java, for example, the optimized parameters
570 greatly improved the model's predictions, but we can also see that the temporal variability in the predictions stays the same although not as pronounced. We noticed this "temporal variability preserving" behavior for several sites such as Beijing, California, Cuttack, New Delhi, Florida, Japan, Michigan, Minnesota, Salmisuo, Texas, and Vercelli. Compared to the case where we optimized only five parameters, the solution for Alberta has improved and the RMSE values for all three trials are
575 for the $d = 11$ case better than the default RMSE value. On the other hand, the solution for Central Java is worse for T1 in the $d = 11$ case than in the $d = 5$ case.

The temporal variability in the model's predictions does not necessarily follow the temporal variability in the observation data (see, for example, Figure 10). Note that in Figure 10 the temporal
580 variability is the same for each of the three trials although the best solutions found in the three trials were very different (see Table 7). Thus, it seems that the improvement of the model's predictions is restricted by an underlying model component that enforces the temporal variability. This is likely to be associated with structural errors either in the methane or in the carbon model. Notice that the methane emission is dependent on the temporal variability predicted in the carbon and land model,
585 especially on the heterotrophic respiration rate, which could have the wrong magnitude or temporal evolution.

Figure 11 shows a scatter plot of the mean values of the CH₄ predictions using default and optimized parameter values versus the mean values of the observed CH₄ emissions. Ideally, if the
590 simulated emissions agreed with the observations, all points would lie on the dashed line. Thus, the closer a point to the dashed line, the more simulation and observation are in agreement. The figure shows that with the optimized parameters, we obtain better or similar results for Beijing, Cuttack, Minnesota, Central Java, Nanjing, Japan, Salmisuo, Alberta, and Michigan. Although not all sites have been strictly improved by the optimization, the overall RMSE has been improved (indicated in
595 the legend).

Figure 11 also shows that with default parameters, CLM4.5bgc predicts less CH₄ emissions than observed for both observation sites in the northern latitudes (Alberta (ID=1) and Salmisuo (ID=16)), which is corrected by the optimization such that the mean emissions at these sites are closer to

600 the dashed line. Thus, based on the observation data, CLM4.5bgc with default parameters does not predict enough emissions in the northern latitudes. On the other hand, CLM4.5bgc over-predicts the emissions for four locations, namely Cuttack (ID=14), Central Java (ID=12), Nanjing (ID=5), and Japan (ID=8), which are located in the tropical/subtropical zone. For those four locations, the predictions with the optimized parameters are closer in agreement with the observations. Hence, the
605 observation data force the model predictions to increase in the northern latitudes and to decrease in the tropics. This can also be seen in Figures 12 and 13 in the following section where we simulated the model globally and compared default and optimized model predictions for the individual zones (discussed below).

5.2.3 Global CH₄ Emission Simulations

610 We simulated CLM4.5bgc to obtain predictions for the CH₄ emissions on a global scale and compared the predictions when using the default parameter values and the optimized parameter values from the 11-dimensional cases. Figure 12 shows spatial plots of the average methane emissions (mg CH₄ m⁻² d⁻¹) and the zonal means (right hand side of the plots) when using the default parameters (panel a), and the difference between the predictions when using the default and the optimized
615 parameters for trial T1 (panel b). The figure shows that with the optimized parameters, the CH₄ emission predictions in the northern regions are larger than for the default parameters. For the tropics, the predictions with the optimized parameters are lower than when using the default values.

Figure 13 shows a comparison of the CH₄ emission predictions from several different models
620 (models 1-10). We can see that globally the predictions with the optimized parameters (model 12) were only slightly higher than with the default parameters (model 11). However, the predictions of CH₄ emissions in the tropics are significantly lower than for the default model and the predictions are also lower in comparison to all other models (1-10). On the other hand, for the northern latitudes, CLM4.5bgc with optimized parameters predicts significantly more CH₄ emissions than the default
625 model and models 1-10 in the comparison. Hence, even though the global average of predicted emissions did not change much, the distribution of the predicted emissions between the tropical and the northern latitudes changed significantly.

As indicated in the previous section, the observation data drives the model to predict more CH₄
630 emissions in northern latitudes and fewer emissions in the tropics. We investigated whether our weighting scheme in equation (1a) may give too much influence to individual observation sites or zones. Thus, we did an additional optimization trial of the parameters in Table 2 where we give each observation site the same weight $w_i = 1$, $i = 1, \dots, 16$ (“unweighted”). We also did a second additional optimization trial of the parameters in Table 2 where we give each zone the same influence
635 on the total RMSE in order to account for the location of the various observation sites (“zonally

weighted”). Thus, each location in the temperate zone (12 sites totally) has $w_i = 1/36$, and each location in the northern (2 sites) and tropical (2 sites) zone, respectively, has the weight $w_i = 1/6$.

The spatial plots of the differences between the average methane emissions when using default
640 and optimized parameters for the unweighted trial are shown in panel (c) of Figure 12, and the spa-
tial plots of the differences when using the zonally weighted objective function is shown in panel
(d) of Figure 12. The figures show that for both additional trials, the CH₄ emissions in the northern
latitudes is even further increased. Moreover, the bars for models 13 and 14 in Figure 13 show the
total methane emissions of the unweighted and the zonally weighted trials, respectively. The zonally
645 weighted trial increases the global emissions, which is caused by larger emission predictions in the
temperate zone and the northern latitudes. In comparison to the default CLM4.5bgc predictions, the
unweighted trial shows a decrease in the predicted emissions in the tropics and an increase in the
predicted emissions in the northern latitudes. Thus, even though it is suggested that CLM4.5bgc with
default parameter settings over-predicts the CH₄ emissions in high latitudes (Koven et al., 2013), the
650 observation data argues that the predictions should even be increased.

6 Conclusions

In this paper we used a surrogate optimization approach for calibrating the parameters of the methane
module of the Community Land Model (CLM4.5bgc). Given only relatively few measurements at
655 16 observation sites (wetlands and rice paddies) our goal was to explore the use of a surrogate op-
timization method to improve the model prediction capability in a computationally efficient way
by minimizing the root mean squared error between the measurements and the model’s predictions.
We identified important methane-related parameters in CLM4.5bgc by doing a sensitivity analysis
and we were thus able to reduce the problem dimension from 21 to 11. We then used a surrogate
660 optimization approach for tuning the most important parameters in order to solve the problem. We
investigated two cases, namely a problem with 5 of the most important parameters and a problem
with all 11 parameters, respectively.

We first used pseudo data in order to asses how well the surrogate optimization performs and
665 showed that we are able to closely match the pseudo observations. We were able to reduce the RMSE
to less than a fifth within the first 150 function evaluations for both pseudo data cases. The objective
function was shown to have multiple local minima, which indicates that the problem is probably
not identifiable when 11 parameters were optimized. Although the RMSE was greatly reduced by
the optimization for the 11 parameter pseudo data case, the optimization results did not generate the
670 same values of the parameters in some cases as were used to generate the pseudo data. This is a

problem with the model, not with the optimization method used. The multiple local minima detected in Table 5 indicate that a global optimization method was needed. We used a surrogate global optimization method because the objective function was expensive to evaluate and has multiple local minima. The surrogate has been shown to reduce the number of objective function evaluations (e.g. 675 climate model simulations) required to obtain accurate approximations of the global minimum and so it is designed for computationally expensive models like climate modules.

By conducting the simulations globally and comparing the average predicted emissions with default and optimized parameters, we could show that the total global CH₄ emissions did not change significantly. However, the distribution of the predicted emissions between latitudes changed significantly. 680 The observation data force the optimized model's CH₄ emission predictions in the northern latitudes to increase and the predicted emissions in the tropics to decrease. In comparison to other models, CLM4.5bgc with both default and optimized parameters predicts significantly more emissions in the northern latitudes and less emissions in the tropics.

Appendix A: Model Equations

685 The methane biogeochemical model used in this study is integrated in the Community Land Model
 version 4.5 (CLM4.5), which is the land component of the Community Earth System Model (CESM,
 Hurrell et al. (2013)). As discussed in more detail in Riley et al. (2011) and Meng et al. (2012), the
 model represents five primary processes relevant to methane emission predictions. These processes
 include methane production (P), oxidation (R_{oxic}), ebullition (E), transport through wetland plant
 690 aerenchyma (A), and diffusion through soil (FD_e) (described below). The methane gas and aqueous
 phase concentrations (R_C) in each soil layer of each grid box is calculated at every time point using
 the following equation:

$$\frac{\partial R_C}{\partial t} = \frac{\partial FD_e}{\partial z} + P - E + A - R_{\text{oxic}} \quad (\text{A1})$$

In the following sections we consider each of these terms in more detail.

695 A1 Methane Production

Methane production (P) in the anaerobic portion of the soil column is related to the grid cell estimate
 of heterotrophic respiration from soil and litter corrected for various factors:

$$P = R_H \cdot F_{\text{CH4}} \cdot Q_{10\text{CH4}} \cdot f_{\text{pH}} f_{\text{pE}} S, \quad (\text{A2})$$

where R_H is the heterotrophic respiration from soil and litter ($\text{mol C m}^{-2} \text{ s}^{-1}$), and F_{CH4} is
 700 the baseline fraction of anaerobically mineralized C atoms becoming CH_4 (i.e., CO_2/CH_4). R_H is
 corrected for its soil temperature dependence through a Q10 factor ($Q_{10\text{CH4}}$), pH (f_{pH}), redox po-
 tential (f_{pE}), and a factor accounting for the seasonal inundation fraction (S).

We adjusted the fractional inundation in each grid cell to account for a changing redox potential.

$$705 f_{\text{pE}} = \frac{f_{i_{\text{lag}}}(t)}{f_i(t)}, \quad (\text{A3})$$

where the redox potential factor f_{pE} is computed based on the fractional inundation $f_i(t)$ and the
 adjusted fractional inundation $f_{i_{\text{lag}}}(t)$ that is producing methane.

The adjusted fractional inundation $f_{i_{\text{lag}}}(t)$ is computed as

$$710 f_{i_{\text{lag}}}(t) = f_i(t) - f_{\text{redox}}(t), \quad (\text{A4})$$

where

$$f_{\text{redox}}(t) = f_i(t) - f_i(t-1) + f_{\text{redox}}(t-1) \left(1 - \frac{\Delta t}{\text{REDOXLAG}} \right) \quad (\text{A5})$$

is the fraction of the grid cell where alternative electron acceptors (such as O_2 , NO_3^- , Fe^{+3} , SO_4^{2-} etc.) are consumed (methane production is completely inhibited), Δt is the time step, and RE-
 715 DOXLAG is the time constant parameter.

In the non-inundated fraction of a grid cell, we estimated the delay in methane production as the water table depth increases by estimating an effective depth below which CH_4 production can occur ($Z_{i_{lag}}$):

$$720 \quad Z_{i_{lag}}(t) = Z_i(t) - Z_{redox}(t), \quad (A6)$$

where

$$Z_{redox}(t) = Z_i(t) - Z_i(t-1) + Z_{redox}(t-1) \left(1 - \frac{\Delta t}{REDOXLAG} \right) \quad (A7)$$

is the depth of the saturated water layer where alternative electron acceptors are consumed at time t and $Z_i(t)$ is the actual water depth at time t .

725

Additionally, we constrained the methane production using the soil pH function f_{pH} which is represented as

$$f_{pH} = 10^{-0.2335pH^2 + 2.7727pH - 8.6}, \quad (A8)$$

730 where pH represents the soil pH. f_{pH} is bounded by two parameters, namely PHMIN and PHMAX (i.e., $PHMIN < pH < PHMAX$). The maximum methane production occurs at $pH \approx 6.2$.

We used a scaling factor (S) to mimic the impacts of seasonal inundation on methane production which is represented as

$$S = \frac{MINO2LIM(f - \bar{f}) + \bar{f}}{f}, \quad S \leq 1, \quad (A9)$$

735 where f and \bar{f} are the instantaneous inundation fraction and annual average inundation fraction weighted by heterotrophic respiration, MINO2LIM is the anoxia factor that relates the fully anoxic decomposition rate to the fully oxygen-unlimited decomposition rate.

A2 Methane Oxidation

Methane oxidation (R_{oxic}) is represented with double Michaelis-Menten kinetics:

$$740 \quad R_{oxic} = VMAX_CH4_OXID \left[\frac{C_{CH_4}}{K_M + C_{CH_4}} \right] \left[\frac{C_{O_2}}{K_M_O2 + C_{O_2}} \right] Q10_CH4OXID \cdot F_{\vartheta}, \quad (A10)$$

where VMAX_CH4_OXID is the maximum oxidation rate ($mol\ m^{-3}\ s^{-1}$), Q10_CH4OXID is the temperature dependence of the reaction, K_M and K_M_O2 are the half saturation coefficients with

respect to CH_4 and O_2 concentrations (mol m^{-3}), C_{CH_4} and C_{O_2} are the methane and oxygen concentrations in the soil (mol m^{-3}), and F_{ϑ} is the soil moisture limitation factor for oxidation applied
745 above the water table to represent water stress for methanotrophs.

F_{ϑ} is represented as:

$$F_{\vartheta} = \exp \left\{ \frac{-P}{P_C} \right\}, \quad (\text{A11})$$

where P and P_C are the soil moisture potential and optimum water potential (-2.4×10^5 mm).
750 If the soil layer is above the water table, the soil moisture limitation factor F_{ϑ} is applied. To account for high- CH_4 -affinity methanotrophs in upland soils, we used a lower oxidation rate constant (VMAX_OXID_UNSAT) and half saturation coefficient with respect to CH_4 concentrations (K_M_UNSAT).

A3 Methane Transport Through Plant Aerenchyma

755 The diffusive transport through aerenchyma A ($\text{mol m}^{-2} \text{s}^{-1}$) from each soil layer is represented in the model as:

$$A = \frac{C(z) - C_a}{r_a + \frac{\text{ROB} \cdot z}{DpT\rho_f}}, \quad (\text{A12})$$

where D is the free-air gas diffusion coefficient ($\text{m}^2 \text{s}^{-1}$), $C(z)$ and C_a are the gaseous concentrations at depth z and at the atmosphere (mol m^{-3}), r_a is the aerodynamic resistance between the
760 surface and the atmospheric reference height (s m^{-1}), ROB is the ratio of root length to vertical depth (obliquity), p is the porosity, T is the specific aerenchyma area ($\text{m}^2 \text{m}^{-2}$), and ρ_f is the root density as a function of depth. Oxygen concentrations can also diffuse into the soil layer from the atmosphere via the reverse of the CH_4 pathway.

765 Here, aerenchyma porosity is parameterized based on the plant functional types (PFTs). A ratio is used to multiply upland vegetation aerenchyma porosity by comparing to inundated systems:

$$p = p \cdot \text{UNSAT_AERE_RATIO} \quad (\text{A13})$$

If the PFT is c3_arctic_grass, c3_nonarctic_grass, or c4_grass, then $p = 0.3$. For the remaining PFTs, the porosity is multiplied by NONGRASSPOROSRATIO (ratio of root porosity in non-grass to
770 grass):

$$p = p \cdot \text{NONGRASSPOROSRATIO}. \quad (\text{A14})$$

A minimum aerenchyma porosity is set to 0.05. Therefore, p is modified as:

$$p = \max\{p, \text{POROSMIN}\}. \quad (\text{A15})$$

The aerenchyma area varies over the course of the growing season. Therefore, it is parameterized using the simulated leaf area index as

$$T = \frac{f_N N_a L}{0.22} \pi R^2, \quad (\text{A16})$$

where L is the leaf area index ($\text{m}^2 \text{m}^{-2}$) (used from CLM4.5 model simulation), N_a is the maximum annual net primary production (NPP, $\text{mol m}^{-2} \text{s}^{-1}$), R is the aerenchyma radius ($2.9 \times 10^{-3} \text{ m}$), and f_N is the below-ground fraction of the current NPP.

780

The aerenchyma area T is multiplied by a scale factor to adjust it:

$$T = T \cdot \text{SCALE_FACTOR_AERE}. \quad (\text{A17})$$

The default value is 1.

A4 Methane Ebullition

785 The representation of the ebullition fluxes in the methane model is based on Wania et al. (2010). The simulated aqueous CH_4 concentration in each soil level is used to estimate the expected equilibrium gaseous partial pressure as a function of temperature and pressure. When this partial pressure exceeds VGC_MAX, bubbling occurs to remove CH_4 to below this value, modified by the fraction of CH_4 in the bubbles (taken as 57%). The VGC_MAX parameter is the ratio of saturation pressure triggering ebullition.

790

A5 Aqueous and Gaseous Diffusion

Gaseous diffusivity in the soil depends on several factors such as molecular diffusivity, soil structure, porosity, and organic matter content. The relationship between effective diffusivity (D_e , $\text{m}^2 \text{s}^{-1}$) and soil properties is represented as

$$795 \quad D_e = D_0 \theta_a^2 \left(\frac{\theta_a}{\theta_s} \right)^{\frac{3}{b}} \cdot \text{SCALE_FACTOR_GASSDIFF}, \quad (\text{A18})$$

where θ_a and θ_s are the air-filled and saturated water-filled porosity, b is the slope of the water retention curve, and SCALE_FACTOR_GASSDIFF is the scale factor for the gas diffusion (the default value is 1).

Appendix B: Observation Sites

800 Tables B1 and B2 show the information about the wetland and rice paddy observation sites, respectively, where methane emissions have been measured.

Appendix C: Parameters and References for Bounds

Table C1 shows the CH₄ related parameters in CLM4.5b_{gc} and their literature reference information.

Appendix D: Weights Used for RMSE Computation in Equation (1) of the Manuscript

805 Table D1 contains information about the weights used for each observation site when computing the
objective function value.

Acknowledgements. The authors want to acknowledge the funding sources DOE SciDAC DE-SC0006791, NSF
1049031, NSF 1049033, and NSF CISE 1116298. The first author also wants to acknowledge partial support by
the U.S. Department of Energy, Office of Science, Office of Advanced Scientific Computing Research, Applied
810 Mathematics program under contract number DE-AC02005CH11231. We thank the anonymous reviewers for
their helpful comments and improvement suggestions.

References

- Adhya, T., Bharati, K., Mohanty, S., Ramakrishnan, B., Rao, V., Sethunathan, N., and Wassmann, R.: Methane emission from rice fields at Cuttack, India, *Nutrient Cycling in Agroecosystems*, 58, 95–105, 2000.
- 815 Aleman, D., Romeijn, H., and Dempsey, J.: A response surface approach to beam orientation optimization in intensity modulated radiation therapy treatment planning, *INFORMS Journal on Computing*, 21, 62–76, 2009.
- Arah, J. and Stephen, K.: A model of the processes leading to methane emission from peatland, *Atmospheric Environment*, 32, 3257–3264, 1998.
- 820 Aselmann, I. and Crutzen, P.: Global distribution of natural fresh-water wetlands and rice paddies, their net primary productivity, seasonality and possible methane emissions, *Journal of Atmospheric Chemistry*, 8, 307–358, 1989.
- Baird, A., Beckwith, C., Waldron, S., and Waddington, J.: Ebullition of methane-containing gas bubbles from near surface Sphagnum peat, *Geophysical Research Letters*, 31, DOI: 10.1029/2004GL021157, 2004.
- 825 Bartlett, K. and Harriss, R.: Review and assessment of methane emissions from wetlands, *Chemosphere*, 26, 261–320, 1993.
- Bartlett, K., Crill, P., Bonassi, J., Richey, J., and Harriss, R.: Methane flux from the Amazon River floodplain: Emissions during rising water, *Journal of Geophysical Research*, 95, 16773–16788, 1990.
- Bender, M. and Conrad, R.: Kinetics of CH₄ oxidation in oxic soils exposed to ambient air or high CH₄ mixing ratios, *FEMS Microbiology Ecology*, 101, 261–270, 1992.
- 830 Bloom, A., Palmer, P., Fraser, A., Reay, D., and Frankenberg, C.: Large-Scale Controls of Methanogenesis Inferred from Methane and Gravity Spaceborne Data, *Science*, 327, 322–325, 2010.
- Booker, A., Dennis Jr, J., Frank, P., Serafini, D., Torczon, V., and Trosset, M.: A rigorous framework for optimization of expensive functions by surrogates, *Structural Multidisciplinary Optimization*, 17, 1–13, 1999.
- 835 Bousquet, P., Ciais, P., Miller, J., Dlugokencky, E., Hauglustaine, D., Prigent, C., Van der Werf, G., Peylin, P., Brunke, E., Carouge, C., Langenfelds, R., Lathiere, J., Papa, F., Ramonet, M., Schmidt, M., Steele, L., Tyler, S., and White, J.: Contribution of anthropogenic and natural sources to atmospheric methane variability, *Nature*, 443, 439–443, 2006.
- Butterbach-Bahl, K., Papen, H., and Rennenberg, H.: Impact of gas transport through rice cultivars on methane emission from rice paddy fields, *Plant, Cell & Environment*, 20, 1175–1183, 1997.
- 840 Cao, M., Marshall, S., and Gregson, K.: Global carbon exchange and methane emissions from natural wetlands: Application of a process-based model, *Journal of Geophysical Research*, 101, 14399–14414, 1996.
- Cheng, W., Yagi, K., Akiyama, H., Nishimura, S., Sudo, S., Fumoto, T., Hasegawa, T., Hartley, A., and Megonigal, J.: An empirical model of soil chemical properties that regulate methane production in Japanese rice paddy soils, *Journal of Environmental Quality*, 36, 1920–1925, 2007.
- 845 Ciais, P., Gasser, T., Paris, J., Caldeira, K., Raupach, M., Canadell, J., Patwardhan, A., Friedlingstein, P., Piao, S., and Gitz, V.: Attributing the increase in atmospheric CO₂ to emitters and absorbers, *Nature Climate Change*, 3, 926–930, 2013.
- Cicerone, R., Shetter, J., and Delwiche, C.: Seasonal-variation of methane flux from a California rice paddy, 850 *Journal of Geophysical Research: Oceans*, 88, 1022–1024, 1983.

- Cicerone, R., Delwiche, C., Tyler, S., and Zimmerman, P.: Methane emissions from California rice paddies with varied treatments, *Global Biogeochemical Cycles*, 6, 233–248, 1992.
- Colmer, T.: Long-distance transport of gases in plants: a perspective on internal aeration and radial oxygen loss from roots, *Plant, Cell & Environment*, 26, 17–36, 2003.
- 855 Computational and Information Systems Laboratory: Yellowstone: IBM iDataPlex System (Wyoming-NCAR Alliance), Boulder, CO: National Center for Atmospheric Research. <http://n2t.net/ark:/85065/d7wd3xhc>, 2012.
- Conrad, R.: Control of microbial methane production in wetland rice fields, *Nutrient Cycling in Agroecosystems*, 64, 59–69, 2002.
- 860 Cronk, J. and Fennessy, M.: *Wetland Plants: Biology and Ecology*, Lewis Publishers, Boca Raton, FL., 2001.
- Davis, E. and Ierapetritou, M.: Kriging based method for the solution of mixed-integer nonlinear programs containing black-box functions, *Journal of Global Optimization*, 43, 191–205, 2009.
- Dlugokencky, E., Nisbet, E., Fisher, R., and Lowry, D.: Global atmospheric methane: budget, changes and dangers, *Philosophical Transactions of the Royal Society A*, 369, 2058–2072, 2011.
- 865 Dunfield, P., Knowles, R., Dumont, R., and Moore, T.: Methane production and consumption in temperate and subarctic peat soils: response to temperature and pH, *Soil Biology & Biochemistry*, 25, 321–326, 1993.
- Forrester, A., Sóbester, A., and Keane, A.: *Engineering Design via Surrogate Modelling - A Practical Guide*, Wiley, 2008.
- Friedman, J.: Multivariate Adaptive Regression Splines, *The Annals of Statistics*, 19, 1–141, 1991.
- 870 Giunta, A., Balabanov, V., Haim, D., Grossman, B., Mason, W., Watson, L., and Haftka, R.: Aircraft multidisciplinary design optimisation using design of experiments theory and response surface modelling, *Aeronautical Journal*, 101, 347–356, 1997.
- Goel, T., Haftka, R. T., Shyy, W., and Queipo, N. V.: Ensemble of Surrogates, *Structural Multidisciplinary Optimization*, 33, 199–216, 2007.
- 875 Grunfeld, S. and Brix, H.: Methanogenesis and methane emissions: effects of water table, substrate type and presence of *Phragmites australis*, *Aquatic Botany*, 64, 63–75, 1999.
- Gutmann, H.: A Radial Basis Function Method for Global Optimization, *Journal of Global Optimization*, 19, 201–227, 2001.
- Han, X., Hendricks Franssen, H.-J., Montzka, C., and Vereecken, H.: Soil moisture and soil properties estimation in the Community Land Model with synthetic brightness temperature observations, *Water Resources Research*, 50, 6081–6105, 2014.
- 880 Huang, Y., Jaing, J., Zong, L., Sass, R., and Fisher, F.: Comparison of field measurements of CH₄ emission from rice cultivation in Nanjing, China and in Texas, USA, *Advances in Atmospheric Sciences*, 18, 1121–1130, 2001.
- 885 Hurrell, J., Holland, M., Gent, P., Ghan, S., Kay, J., Kushner, P., Lamarque, J.-F., Large, W., Lawrence, D., Lindsay, K., Lipscomb, W., Long, M., Mahowald, N., Marsh, D., Neale, R., Rasch, P., Vavrus, S., Vertenstein, M., Bader, D., Collins, W., Hack, J., Kiehl, J., and Marshall, S.: The Community Earth System Model: A Framework for Collaborative Research, *Bull. Amer. Meteor. Soc.*, 94, 1339–1360, 2013.

- Jain, M., Kumar, S., Wassmann, R., Mitra, S., Singh, S., Singh, J., Singh, R., Yadav, A., and Gupta, S.: Methane emissions from irrigated rice fields in northern India (New Delhi), *Nutrient Cycling in Agroecosystems*, 58, 75–83, 2000.
- Jiang, C., Wang, Y., Zheng, X., Zhu, B., Huang, Y., and Hao, Q.: Methane and nitrous oxide emissions from three paddy rice based cultivation systems in southwest China, *Advances in Atmospheric Sciences*, 23, 415–424, 2006.
- 895 Jones, D., Schonlau, M., and Welch, W.: Efficient Global Optimization of Expensive Black-Box Functions, *Journal of Global Optimization*, 13, 455–492, 1998.
- Keller, M. M.: Biological Sources and Sinks of Methane in Tropical Habitats and Tropical Atmospheric Chemistry, Ph.D. thesis, Princeton University, 1990.
- Kellner, E., Baird, A., Oosterwoud, M., Harrison, K., and Waddington, J.: Effect of temperature and atmospheric pressure on methane (CH₄) ebullition from near surface peats, *Geophysical Research Letters*, 33, DOI: 10.1029/2006GL027509, 2006.
- 900 Knoblach, C.: Bodenkundlich-mikrobiologische Bestandsaufnahme zur Methanoxidation in einer Flussmarsch der Tide-Elbe, Master's thesis, University of Hamburg, Hamburg, Germany, 1994.
- Koven, C., Riley, W., Subin, Z., Tang, J., Torn, M., Collins, W., Bonan, G., Lawrence, D., and Swenson, S.: The effect of vertically resolved soil biogeochemistry and alternate soil C and N models on C dynamics of CLM4, *Biogeosciences*, 10, 7109–7131, 2013.
- 905 Lo, M.-H., Famiglietti, J., Yeh, P.-F., and Syed, T.: Improving parameter estimation and water table depth simulation in a land surface model using GRACE water storage and estimated base flow data, *Water Resources Research*, 46, W05517, 2010.
- 910 Lombardi, J., Epp, M., and Chanton, J.: Investigation of the methyl fluoride technique for determining rhizospheric methane oxidation, *Biogeochemistry*, 36, 153–172, 1997.
- Matthews, E. and Fung, I.: Methane emission from natural wetlands: global distribution, area, and environmental characteristics of sources, *Global Biogeochemical Cycles*, 1, 61–86, 1987.
- Meng, L., Hess, P., Mahowald, N., Yavitt, J., Riley, W., Subin, Z., Lawrence, D., Swenson, S., Jauhainen, J., and Fuka, D.: Sensitivity of wetland methane emissions to model assumptions: application and model testing against site observations, *Biogeosciences*, 9, 2793–2819, 2012.
- 915 Moore, D., Hub, J., Sacks, W. J., Schimel, D., and Monson, R.: Estimating transpiration and the sensitivity of carbon uptake to water availability in a subalpine forest using a simple ecosystem process model informed by measured net CO₂ and H₂O fluxes, *Agricultural and Forest Meteorology*, 148, 1467–1477, 2008.
- 920 Mugunthan, P., Shoemaker, C., and Regis, R.: Comparison of function approximation, heuristic, and derivative-based methods for automatic calibration of computationally expensive groundwater bioremediation models, *Water Resources Research*, 41, W11427, 2005.
- Müller, J. and Piché, R.: Mixture Surrogate Models Based on Dempster-Shafer Theory for Global Optimization Problems, *Journal of Global Optimization*, 51, 79–104, 2011.
- 925 Müller, J. and Shoemaker, C.: Influence of ensemble surrogate models and sampling strategy on the solution quality of algorithms for computationally expensive black-box global optimization problems, *Journal of Global Optimization*, pp. DOI: 10.1007/s10898-014-0184-0, 2014.

- Müller, J., Shoemaker, C., and Piché, R.: SO-MI: A Surrogate Model Algorithm for Computationally Expensive Nonlinear Mixed-Integer Black-Box Global Optimization Problems, *Computers and Operations Research*, 40, 1383–1400, 2013.
- Myers, R. and Montgomery, D.: *Response Surface Methodology, Process and Product Optimization using Designed Experiments*, Wiley-Interscience Publication, 1995.
- Myhre, G., Shindell, D., Bréon, F.-M., Collins, W., Fuglestedt, J., Huang, J., Koch, D., Lamarque, J.-F., Lee, D., Mendoza, B., Nakajima, T., Robock, A., Stephens, G., Takemura, T., and Zhang, H.: Anthropogenic and Natural Radiative Forcing. In: *Climate Change 2013: The Physical Science Basis. Contribution of Working Group I to the Fifth Assessment Report of the Intergovernmental Panel on Climate Change*, Cambridge University Press, Cambridge, United Kingdom and New York, NY, USA, 2013.
- Oleson, K., Lawrence, D., Bonan, G., Drewniak, B., Huang, M., Koven, C., Levis, S., Li, F., Riley, W., Subin, Z., Swenson, S., Thornton, P., Bozbiyik, A., Fisher, R., Kluzek, E., Lamarque, J.-F., Lawrence, P., Leung, L., Lipscomb, W., Muszala, S., Ricciuto, D., Sacks, W., Sun, Y., Tang, J., and Yang, Z.-L.: Technical Description of Version 4.5 of the Community Land Model (CLM), Tech. Rep. NCAR/TN-503+STR, National Center for Atmospheric Research, Boulder, CO, DOI: 10.5065/D6RR1W7, 2013.
- Popp, T. J., Chanton, J. P., Whiting, G. J., and Grant, N.: Evaluation of Methane Oxidation in the Rhizosphere of Carex Dominated Fen in North Central Alberta, Canada, *Biogeochemistry*, 51, 259–281, 2000.
- Powell, M.: The Theory of Radial Basis Function Approximation in 1990, *Advances in Numerical Analysis*, vol. 2: wavelets, subdivision algorithms and radial basis functions. Oxford University Press, Oxford, pp. 105-210, 1992.
- Prigent, C., Papa, F., Aires, F., Rossow, W., and Matthews, E.: Global inundation dynamics inferred from multiple satellite observations, 1993-2000, *Journal of Geophysical Research*, 112, DOI:10.1029/2006JD007847, 2007.
- Prihodko, L., Denning, A., Hanan, N., Baker, I., and Davis, K.: Sensitivity, uncertainty and time dependence of parameters in a complex land surface model, *Agricultural and Forest Meteorology*, 148, 268–287, 2008.
- Qian, T., Dai, A., Trenberth, K., and Oleson, K.: Simulation of global land surface conditions from 1948 to 2004. Part I: Forcing data and evaluations, *Journal of Hydrometeorology*, 7, 953–975, 2006.
- Ray, J. and Swiler, L.: Bayesian calibration of the Community Land Model using surrogates, Tech. Rep. SAND2014-0867, Sandia National Laboratories, Livermore, CA, 2014.
- Regis, R.: Stochastic radial basis function algorithms for large-scale optimization involving expensive black-box objective and constraint functions, *Computers & Operations Research*, 38, 837–853, 2011.
- Regis, R. and Shoemaker, C.: A Stochastic Radial Basis Function Method for the Global Optimization of Expensive Functions, *INFORMS Journal on Computing*, 19, 497–509, 2007.
- Regis, R. and Shoemaker, C.: Parallel Stochastic Global Optimization Using Radial Basis Functions, *INFORMS Journal on Computing*, 21, 411–426, 2009.
- Regis, R. and Shoemaker, C.: Combining radial basis function surrogates and dynamic coordinate search in high-dimensional expensive black-box optimization, *Engineering Optimization*, 45, 529–555, 2013.
- Riley, W., Subin, Z., Lawrence, D., Swenson, S., Torn, M., Meng, L., Mahowald, N., and Hess, P.: Barriers to predicting changes in global terrestrial methane fluxes: analyses using CLM4Me, a methane biogeochemistry model integrated in CESM, *Biogeosciences Discussions*, 8, doi:10.5194/bgd-8-1733-2011, 2011.

- Ringeval, B., de Noblet-Ducoudre, N., Ciais, P., Bousquet, P., Prigeent, C., Papa, F., and Rossow, W.: An attempt to quantify the impact of changes in wetland extent on methane emissions on the seasonal and interannual time scales, *Global Biogeochemical Cycles*, 24, DOI:10.1029/2008gb003354, 2010.
- 970 Saarnio, S., Alm, J., Silvola, J., Lohila, A., Nykänen, H., and Martikainen, P.: Seasonal Variation in CH₄ Emissions and Production and Oxidation Potentials at Microsites on an Oligotrophic Pine Fen, *Oecologia*, 110, 414–422, 1997.
- Schuh, A., Denning, A., Corbin, K., Baker, I., Uliasz, M., Parazoo, N., Andrews, A., and Worthy, D.: A regional high-resolution carbon flux inversion of North America for 2004, *Biogeosciences*, 7, 1625–1644, 2010.
- 975 Segers, R.: Methane production and methane consumption: a review of processes underlying wetland methane fluxes, *Biogeochemistry*, 41, 23–51, 1998.
- Segers, R. and Kengen, S.: Methane production as a function of anaerobic carbon mineralization: A process model, *Soil Biology & Biochemistry*, 30, 1107–1117, 1998.
- 980 Setyanto, P., Rosenami, A., Boer, R., Fauziah, C., and Khanif, M.: The effect of rice cultivars on methane emission from irrigated rice field, *Indonesian Journal of Agricultural Sciences*, 5, 20–31, 2004.
- Shannon, R. D. and White, J. R.: 3-Year Study of Controls on Methane Emissions from 2 Michigan Peatlands, *Biogeochemistry*, 27, 35–60, 1994.
- Shurpali, N. J. and Verma, S. B.: Micrometeorological measurements of methane flux in a Minnesota peatland during two growing seasons, *Biogeochemistry*, 40, 1–15, 1998.
- 985 Sigren, L., Lewis, S., Fisher, F., and Sass, R. L.: Effects of field drainage on soil parameters related to methane production and emission from rice paddies, *Global Biogeochemical Cycles*, 11, 151–162, 1997.
- Simpson, T., Mauery, T., Korte, J., and Mistree, F.: Kriging metamodelling for global approximation in simulation-based multidisciplinary design optimization, *AIAA Journal*, 39, 2233–2241, 2001.
- 990 Solonen, A., Ollinaho, P., Laine, M., Haario, H., Tamminen, J., and Järvinen, H.: Efficient MCMC for climate model parameter estimation: Parallel adaptive chains and early rejection, *Bayesian Analysis*, 7, 715–736, 2012.
- Subin, Z., Riley, W., and Mironov, D.: Improved lake model for climate simulations, *J. Adv. Model. Earth Syst.*, 4, DOI:10.1029/2011MS000072, 2012.
- 995 Sun, Y., Hou, Z., Huang, M., Tian, F., and Leung, L.: Inverse Modeling of Hydrologic Parameters Using Surface Flux and Runoff Observations in the Community Land Model, *Hydrology and Earth System Sciences*, 17, 4995–5011, 2013.
- Swenson, S. and Lawrence, D.: A New Fractional Snow Covered Area Parameterization for the Community Land Model and its Effect on the Surface Energy Balance, *Journal of Geophysical Research*, 117, DOI:10.1029/2012JD018178, 2012.
- 1000 Swenson, S., Lawrence, D., and Lee, H.: Improved Simulation of the Terrestrial Hydrological Cycle in Permafrost Regions by the Community Land Model, *Journal of Advances in Modeling Earth Systems*, 4, DOI:10.1029/2012MS000165, 2012.
- Thornton, P., Lamarque, J., Rosenbloom, N., and Mahowald, N.: Influence of carbon-nitrogen cycle coupling on land model response to CO₂ fertilization and climate variability, *Global Biogeochemical Cycles*, 21, 2007.
- 1005

- Thornton, P., Doney, S., Lindsay, K., Moore, J., Mahowald, N., Randerson, J., Fung, I., Lamarque, J., Feddema, J., and Lee, Y.-H.: Carbon-nitrogen interactions regular climate-carbon cycle feedbacks: results from an atmosphere-ocean general circulation model, *Biogeosciences-discussion*, 6, 3303–3354, 2009.
- 1010 Tian, X., Xie, Z., and Dai, A.: A land surface soil moisture data assimilation system based on the dual-UKF method and the Community Land Model, *Journal of Geophysical Research: Atmospheres*, 113, D14 127, 2008.
- Turner, D., Ritts, W., Wharton, S., Thomas, C., Monson, R., Black, T., and Falk, M.: Assessing FPAR source and parameter optimization scheme in application of a diagnostic carbon flux model, *Remote Sensing of Environment*, 113, 1529–1539, 2009.
- 1015 Viana, F., Haftka, R., and Steffen Jr., V.: Multiple surrogates: how cross-validation errors can help us to obtain the best predictor, *Structural and Multidisciplinary Optimization*, 39, 439–457, 2009.
- Walter, B. and Heimann, M.: A process-based, climate-sensitive model to derive methane emissions from natural wetlands: Application to five wetland sites, sensitivity to model parameters, and climate, *Global Biogeochemical Cycles*, 14, 745–765, 2000.
- 1020 Walter, B., Heimann, M., and Matthews, E.: Modeling modern methane emissions from natural wetlands 1. Model description and results, *Journal of Geophysical Research: Atmospheres*, 106, 34 189–34 206, 2001.
- Wang, Z., Xu, Y., Li, Z., Guo, Y., Wassmann, R., Neue, H., Lantin, R., Buendia, L., Ding, Y., and Wang, Z.: A four-year record of methane emissions from irrigated rice fields in the Beijing region of China, *Nutrient Cycling in Agroecosystems*, 58, 55–63, 2000.
- 1025 Wania, R., Ross, I., and Prentice, I.: Implementation and evaluation of a new methane model within a dynamic global vegetation model: LPJ-WHyMe v1.3.1, *Geoscientific Model Development*, 3, 565–584, 2010.
- Whalen, S. and Reeburgh, W.: Moisture and temperature sensitivity of CH₄ oxidation in boreal soils, *Soil Biology & Biochemistry*, 28, 1271–1281, 1996.
- Wild, S. and Shoemaker, C.: Global convergence of radial basis function trust-region algorithms for derivative-free optimization, *SIAM Review*, 55, 349–371, 2013.
- 1030 Yagi, K., Tsuruta, H., Kanda, K., and Minami, K.: Effect of water management on methane emission from a Japanese rice paddy field: Automated methane monitoring, *Global Biogeochemical Cycles*, 10, 255–267, 1996.
- Yang, B., Qian, Y., Lin, G., Leun, R., and Zhang, Y.: Some issues in uncertainty quantification and parameter tuning: A case study of convective parameterization in the WRF regional climate model, *Atmospheric Chemistry and Physics*, pp. 2409–2427, 2012.
- 1035 Yang, B., Qian, Y., Lin, G., Leung, L., Rasch, P., Zhang, G., McFarlane, S., Zhao, C., Zhang, Y., Wang, H., Wang, M., and Liu, X.: Uncertainty quantification and parameter tuning in the CAM5 Zhang-McFarlane convection scheme and impact of improved convection on the global circulation and climate, *Journal of Geophysical Research: Atmospheres*, 118, 395–415, 2013.
- 1040 Zeng, X., Drewniak, B., and Constantinescu, E.: Calibration of the Crop Model in the Community Land Model, *Geoscientific Model Development Discussions*, 6, 379–398, 2013.
- Zhang, Y., Li, C., Trettin, C., Li, H., and Sun, G.: An integrated model of soil, hydrology, and vegetation for carbon dynamics in wetland ecosystems, *Global Biogeochemical Cycles*, 16, 1–17, 2002.

- 1045 Zhu, Q., Liu, J., Peng, C., Chen, H., Fang, X., Jiang, H., Yang, G., Zhu, D., Wang, W., and Zhou, X.: Modelling methane emissions from natural wetlands: TRIPLEX-GHG model integration, sensitivity analysis, and calibration, *Geoscientific Model Development Discussions*, 6, 5423–5473, 2013.
- Zhuang, Q., Melillo, J., Kicklighter, D., Prinn, R., McGuire, A., Steudler, P., Felzer, B., and Hu, S.: Methane fluxes between terrestrial ecosystems and the atmosphere at northern high latitudes during the past century: A retrospective analysis with a process-based biogeochemistry model, *Global Biogeochemical Cycles*, 18, DOI: 3010.1029/2004GB002239, 2004.
- 1050

Table 1. CH₄ related parameters in CLM4.5bgc and their upper and lower bounds x_k^u and x_k^l , respectively, and the default parameter values v_k .

Parameter ID	Parameter name	x_k^l	x_k^u	v_k
1	Q10CH4	1	4	1.33
2	F_CH4	0.1	0.4	0.26
3	REDOXLAG	15	45	30
4	OXINHIB	200	600	400
5	PHMAX	8	10	9
6	PHMIN	2	4	2.2
7	VMAX_CH4_OXID	1.25e-6	1.25e-4	1.25e-5
8	K_M	0.0005	0.05	0.005
9	K_M_O2	0.002	0.2	0.002
10	Q10_CH4OXID	1	4	1.9
11	K_M_UNSAT	0.00005	0.005	0.0005
12	VMAX_OXID_UNSAT	1.25e-7	1.25e-5	1.25e-6
13	SCALE_FACTOR_AERE	0.2	2	1
14	NONGRASSPOROSRATIO	0.2	0.5	0.33
15	POROSMIN	0.01	0.2	0.05
16	ROB	2	4	3
17	UNSAT_AERE_RATIO	0.1	0.25	0.1667
18	VGC_MAX	0.05	0.3	0.15
19	SCALE_FACTOR_GASDIFF	1	5	1
20	ATMCH4	1.7e-7	1.7e-5	1.7e-6
21	MINO2LIM	0.1	0.3	0.2

Table 2. Parameters that are sensitive for most observation sites (out of 16).

Parameter ID	Parameter name	# sensitive sites
1	Q10CH4	16
2	F_CH4	16
7	VMAX_CH4_OXID	16
13	SCALE_FACTOR_AERE	16
9	K_M_O2	15
15	POROSMIN	14
16	ROB	11
8	K_M	10
17	UNSAT_AERE_RATIO	10
10	Q10_CH4OXID	9
21	MINO2LIM	9

Table 3. Parameters that are least sensitive for observation sites (out of 16).

Parameter ID	Parameter name	# insensitive sites
3	REDOXLAG	16
4	OXINHIB	16
5	PHMAX	16
6	PHMIN	16
14	NONGRASSPOROSRATIO	16
18	VGC_MAX	16
20	ATMCH4	15
11	K_M_UNSAT	13
19	SCALE_FACTOR_GASDIFF	13
12	VMAX_OXID_UNSAT	10

Table 4. Default and optimized parameter values of optimization trials T1, T2, and T3 for the 5-dimensional pseudo data case. We report four decimal places because the model output is sensitive to very small changes for some variables. Note that we scaled the numbers to the interval [0,1].

Param.	Default	T1	T2	T3
1	0.1100	0.1088	0.1099	0.1091
2	0.5333	0.5366	0.5385	0.5458
7	0.0909	0.0912	0.0943	0.0967
13	0.4444	0.4461	0.4454	0.4443
21	0.5000	0.4936	0.4934	0.4856
RMSE	0	0.28	0.46	0.40

Table 5. Default and optimized parameter values of optimization trial T3 and parameter values for the point CP that was sampled during the same optimization trial and that is closer to the default point, but that has a worse objective function value (11-dimensional pseudo data case).

Param.	Default	T3	CP
1	0.1100	0.1148	0.1148
2	0.5333	0.5806	0.5806
7	0.0909	0.1336	0.1336
8	0.0909	0.1785	0.1785
9	0.0909	0.1248	0.1248
10	0.3000	0.4375	0.4302
13	0.4444	0.7107	0.7107
15	0.2105	0.1778	0.1778
16	0.5000	0.9583	0.9583
17	0.4444	0.2740	0.2740
21	0.5000	0.4436	0.4583
RMSE	0	2.28	2.35

Table 6. Default and optimized parameter values of optimization trials T1, T2, and T3 for the 5-dimensional real data case. Bold indicates optimized parameters that are on (or close to) the variable boundary (all variables are scaled to [0,1]).

Param.	Default	T1	T2	T3
1	0.1100	0	0	0
2	0.5333	0.1705	0.1747	0.1699
7	0.0909	0.7878	0.7518	0.7865
13	0.4444	0	0	0.0267
21	0.5000	1	1	1
RMSE	156.40	114.24	114.11	114.24

Table 7. Default and optimized parameter values of optimization trials T1, T2, and T3 for the 11-dimensional real data case. Bold indicates optimized parameters that are on the variable bound (all variables are scaled to [0,1]).

Param.	Default	T1	T2	T3
1	0.1100	0	0	0
2	0.5 333	0.4220	0.3298	0.3813
7	0.0909	0.7093	0.6889	0.7260
8	0.0909	1	1	0.9754
9	0.0909	0	0.2335	0.6971
10	0.3000	0.7702	0.6195	0.6195
13	0.4444	1	1	0.8063
15	0.2105	0.6987	1	1
16	0.5000	0.0865	0.4274	0.2473
17	0.4444	0.8543	0.3113	0.5359
21	0.5000	0.5064	0.7449	0.5586
RMSE	164.46	107.24	107.58	107.41

Table 8. Unweighted RMSE values for each site using the best parameters found during optimization trial T1 of the $d = 11$ real data case and trial T2 of the $d = 5$ real data case and with default parameter values.

Site	Name	Unweighted RMSE $d = 5$	Unweighted RMSE $d = 11$	Unweighted RMSE default
1	Alberta	220.34	203.82	209.25
2	Florida	1247.70	1280.29	1180.99
3	Michigan	334.01	337.51	328.10
4	Minnesota	41.05	35.16	34.31
5	Nanjing	97.88	96.14	212.18
6	Vercelli	325.34	326.04	293.36
7	Texas	179.21	139.09	116.85
8	Japan	132.31	161.22	184.88
9	California	372.71	374.59	360.37
10	New Delhi	18.67	19.96	14.21
11	Beijing	66.79	60.89	56.99
12	Java	49.09	54.61	221.52
13	Chengdu	231.93	241.91	198.42
14	Cuttack	72.01	63.75	364.75
15	Panama	446.83	464.59	422.86
16	Salmisuo	156.79	132.16	146.52
Total RMSE		3792.66	3991.73	4345.56

Table B1. Wetland site data. P = precipitation, T = temperature

Site Name	Location	Time	Wetland type	Dominant vegetation	Mean P & T	Soil and climate characteristics	Meas. techniques	Forcing datasets*	References
Michigan, USA	42.45 N, 84.00 E	1991 - 1993	Ombrotrophic peatland	Sphagnum, Scheuchzeria palustris, Vaccinium oxycoccus	P: 761mm (1948-1980)	Soil pH: 4.2	Static chamber	Measured positions	Shannon and White (1994)
Minnesota, USA	47.53 N, 266.33 E	1991 - 1992	Poorly minerotrophic to ombrotrophic peatland	Sphagnum, Chamaedaphne calyculata, Scheuchzeria palustris	P: 553mm, T: $\approx 13.6^{\circ}\text{C}$ for May-October period	Soil pH: 4.6	Eddy correlation technique	Measured positions	Shurpali and Verma (1998)
Alberta, Canada	54.60 N, 246.60 E	1994 - 1996	Nutrient rich fen	Carex aquatilis and Carex rostrata	-	Soil pH: 7; the freeze-thaw cycle spans from May to Oct	Open chamber	Measured positions	Popp et al. (2000)
Salmisuo, Eastern Finland	62.75 N, 30.93 E	1993	Minerotrophic oligotrophic pine fen	Sphagnum papillosum	T: $\approx 10^{\circ}\text{C}$	Wet condition from Jul to Sept	Static chamber	Measured positions	Saarnio et al. (1997)
Florida, USA	30.07 N, 275.80 E	1993	Swamp	Sagittaria lancifolia	Annual P: $\approx 1400\text{mm}$	Soil pH: 6.2	Open chamber	Measured positions	Lombardi et al. (1997)
Panama	9.00 N, 80.00 E	1987	Swamp	Palms	-	Soil pH: 6.2; Feb to May is the dry season	Static chamber	Modeled WT positions	Keller (1990); Walter and Heimann (2000)

Table B2. Rice paddy site data

Site Name	Location	Year	Date of Field flooded	Date of final drainage	pH	Measurement techniques	Soil type	References
Texas, USA	29.95 N, 265.50 E	1994	17-May	11-Aug	N/A	Chamber	Bernard-Morey	Sigren et al. (1997)
Vercelli, Italy	45.30 N, 8.42 E	1991	7-May	30-Aug	6	Static chamber	Sandy loam	Butterbach-Bahl et al. (1997)
Chengdu, China	31.27 N, 105.45 E	2003	9-May	7-Sep	8.1	Chamber	Purplish	Jiang et al. (2006)
Nanjing, China	32.80 N, 118.75 E	1999	18-Jun	13-Oct	N/A	Chamber	Hydromorphic	Huang et al. (2001)
Beijing, China	40.55 N, 116.78 E	1995	4-Jun	17-Oct	7.99	Automatic chamber	Silty clay loam	Wang et al. (2000)
California, USA	40.20 N, 237.98 E	1982&1983	11-May (1982); 21-May (1983)	1-Oct (1982); 1-Oct (1983)	N/A	Static chamber	Capay silty clay	Cicerone et al. (1992, 1983)
Japan	36.02 N, 140.22 E	1991&1993	7-May	12-Aug (1991); 2-Sept (1993)	6.6-6.9	Automatic chamber	Gley soil (Sandy clay loam)	Yagi et al. (1996)
New Delhi, India	28.63 N, 77.12 E	1995	1-Jul	1-Nov	8.2	Closed chamber, manual	Ustochrept (sandy loam)	Jain et al. (2000)
Cuttack, India	20.42 N, 85.92 E	1996	19-Jul	30-Oct	6.19	Automatic chamber	Haplaquept (Al-luvial)	Adhya et al. (2000)
Central Java, Indonesia	6.78 S, 110.15 E	2001-2002	1-Nov	28-Feb	5.1	Automatic closed chamber	Aeric Tropaquept (Silty loam)	Setyanto et al. (2004)

Table C1. Parameter names, descriptions, ranges, and literature references

Number	Parameter	Description	Units	Range	References
1	q10ch4	Q10 for methane production	unitless	1 - 10	Dunfield et al. (1993); Walter and Heimann (2000); Riley et al. (2011)
2	f_ch4	Ratio of CH ₄ production to total C mineralization	unitless	0.05 - 0.5	Wania et al. (2010); Zhang et al. (2002); Zhu et al. (2013), Effective value will depend on temperature, redox and pH but cannot exceed 50% based on stoichiometry (Bill Riley, personal communication)
3	redoxlag	Number of days to lag for production	days	15 - 45	Meng et al. (2012); Conrad (2002); Cheng et al. (2007)
4	oxinhib	Inhibition of methane production by oxygen	m ³ /mol	200 - 600	Arah and Stephen (1998); Riley et al. (2011)
5	pHmax	Maximum pH for methane production	unitless	8 - 10	Cao et al. (1996); Zhang et al. (2002); Zhuang et al. (2004); Meng et al. (2012)
6	pHmin	Minimum pH for methane production	unitless	2 - 4	Cao et al. (1996); Zhang et al. (2002); Zhuang et al. (2004); Meng et al. (2012)
7	vmax_ch4_oxid	Oxidation rate constant	mol/m ³ -w/s	1.25e-6 - 1.25e-4	Riley et al. (2011); Walter and Heimann (2000); Dunfield et al. (1993); Knoblauch (1994)
8	k_m	Michaelis-Menten oxidation rate constant for CH ₄ conc.	mol/m ³ -w	5e-4 - 5e-2	Segers and Kengen (1998); Walter and Heimann (2000); Riley et al. (2011)
9	k_m_o2	Michaelis-Menten oxidation rate constant for O ₂ conc.	mol/m ³ -w	0.002 - 0.2	Segers (1998); Walter and Heimann (2000); Riley et al. (2011)
10	q10_ch4oxid	Q10 oxidation constant	unitless	1 - 4	Meng et al. (2012); ?; Walter and Heimann (2000); Zhu et al. (2013); Zhang et al. (2002)
11	k_m_unsat	Michaelis-Menten oxidation rate constant for CH ₄ conc. in upland areas	mol/m ³ -w	5e-5 - 5e-3	Whalen and Reeburgh (1996); Bender and Conrad (1992); Riley et al. (2011)
12	vmax_oxid_unsat	Oxidation rate constant in upland areas	mol/m ³ -w/s	1.25e-7 - 1.25e-5	Whalen and Reeburgh (1996); Bender and Conrad (1992); Riley et al. (2011)
13	scale_factor_aere	Scale factor on the aerenchyma area	unitless	0.2 - 5	Riley et al. (2011)
14	nongrassporosratio	Ratio of root porosity in non-grass to grass	unitless	0.2 - 0.5	Colmer (2003)
15	porosmin	Minimum aerenchyma porosity	unitless	0.01 - 0.2	Colmer (2003); Cronk and Fennessy (2001)
16	rob	Ratio of root length to vertical depth ("root obliquity")	unitless	2 - 4	Arah and Stephen (1998); Riley et al. (2011). This parameter is poorly constrained.
17	unsat_aere_ratio	Ratio to multiply upland vegetation aerenchyma porosity by compared to inundated systems	unitless	0.1 - 0.25	Not available in literature. The reasonable range could be between 0.1 and 0.25. Meng et al. (2012) used this range for sensitivity.
18	vgc_max	Ratio of saturation pressure triggering ebullition	unitless	0.05 - 0.3	Kellner et al. (2006); Baird et al. (2004)
19	scale_factor_gasdiff	Scale factor for gas diffusion	unitless	1 - 5	Range not available. Reasonable range is 1-5 for sensitivity analyses.
20	atmch4	Atm. CH ₄ mixing ratio to prescribe	mol/mol	1.7e-7 - 1.7e-5	Range not available. Variable range; global average is $\approx 1.7e-6$
21	mino2lim	Min. anaerobic decomposition rate as a fraction of potential aerobic rate	unitless	0.05 - 0.45	Range not available in the literature. The default value (0.2) is from Riley et al. (2011). The reasonable range could be between 0.05 and 0.45 to adjust effect of anoxia on decomposition rate (used to calculate seasonal inundation factor). The range is considered based on knowledge.

Table D1. ID, name of observation sites, and associated weights for real data and pseudo data case (equation (1) of the main document)

ID	Location	w_i real data	w_i pseudo data
1	Alberta	0.0327	0.0656
2	Florida	0.0078	0.0067
3	Michigan	0.0280	0.1599
4	Minnesota	0.0938	0.0783
5	Nanjing	0.0566	0.0149
6	Vercelli	0.0198	0.0382
7	Texas	0.0267	0.0189
8	Japan	0.0441	0.0153
9	California	0.0421	0.0684
10	New Delhi	0.2787	0.1707
11	Beijing	0.1053	0.1189
12	Central Java	0.0810	0.0143
13	Chengdu	0.0283	0.0571
14	Cuttack	0.0968	0.0104
15	Panama Swamp	0.0177	0.0795
16	Salmisuo	0.0405	0.0827

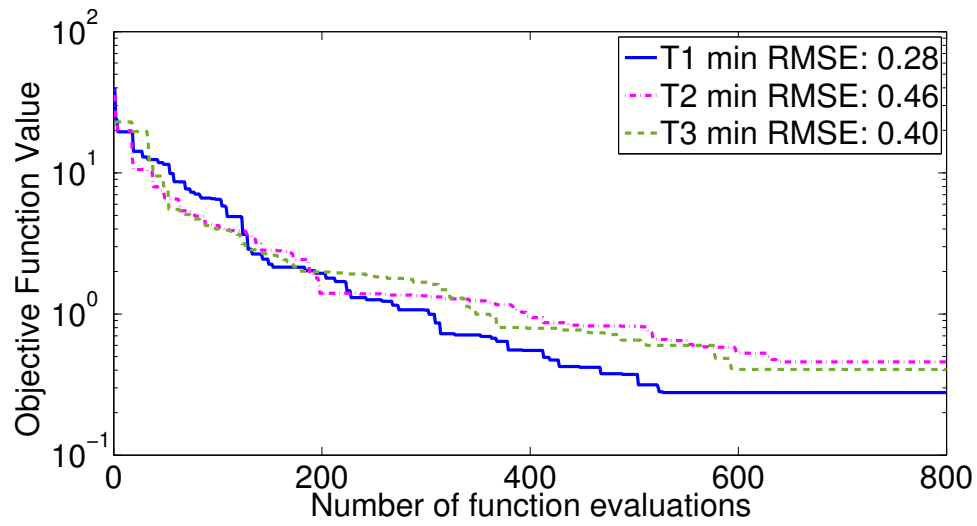


Figure 1. Progress plot that shows the development of the best objective function value found versus the number of function evaluations for the pseudo data case with $d = 5$ parameters for optimization trials T1, T2, and T3. The legend shows the lowest RMSE value found in each trial.

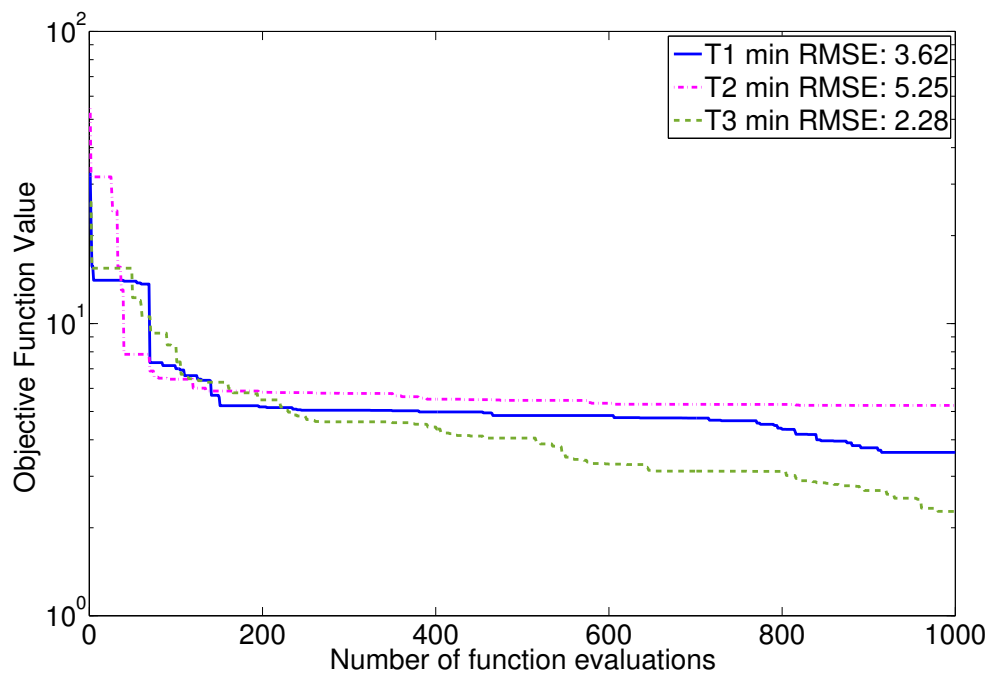


Figure 2. Progress plot that shows the development of the best objective function value found versus the number of function evaluations for the pseudo data case with $d = 11$ parameters for optimization trials T1, T2, and T3. The legend shows the lowest RMSE value found in each trial.

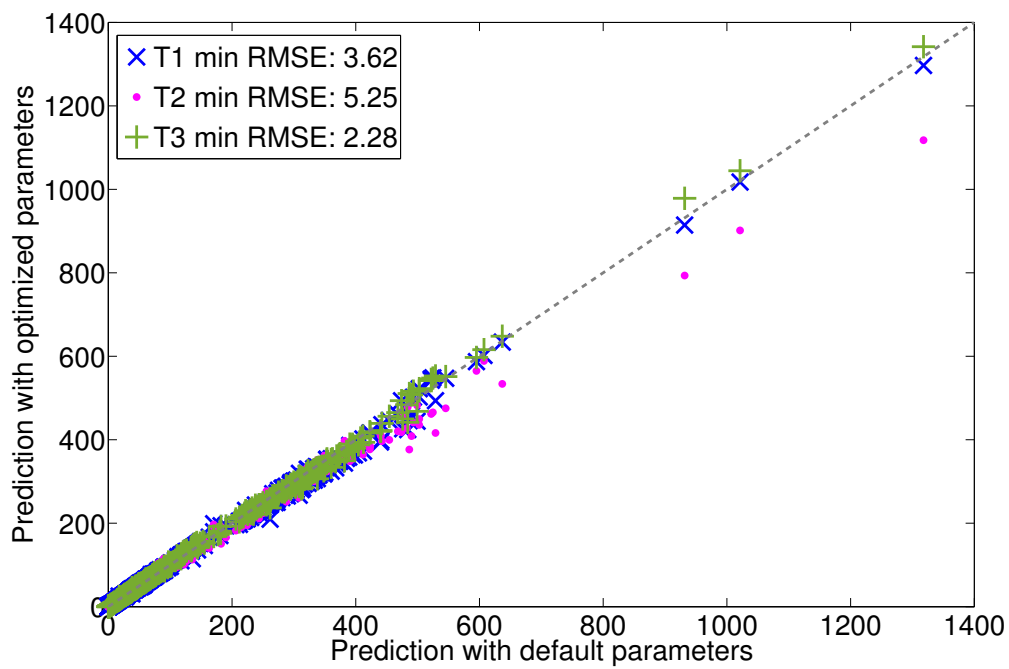


Figure 3. CLM4.5bgc CH₄ predictions when using the default parameter values versus the predictions when using the best solution found in each of the three optimization trials T1, T2, and T3, respectively, for the pseudo data case with $d = 11$ parameters. The legend shows the lowest RMSE value found in each trial.

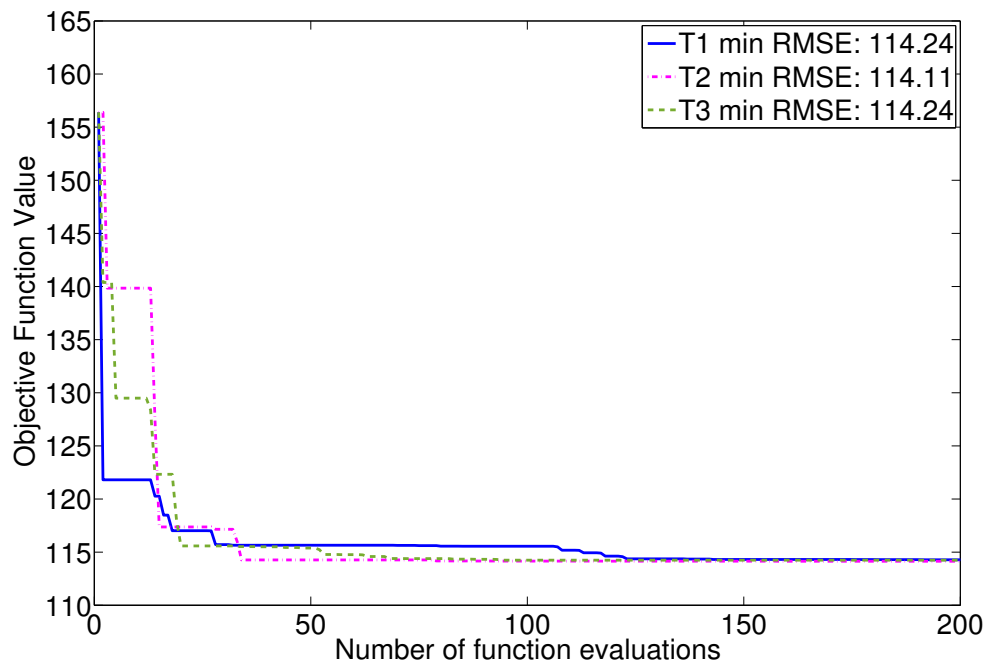


Figure 4. Progress plot that shows the development of the best objective function value found versus the number of function evaluations for the real data case with $d = 5$ parameters for optimization trials T1, T2, and T3. The legend shows the lowest RMSE value found in each trial. The first function evaluation (left side of the graphs) corresponds to the RMSE when using the default parameters.

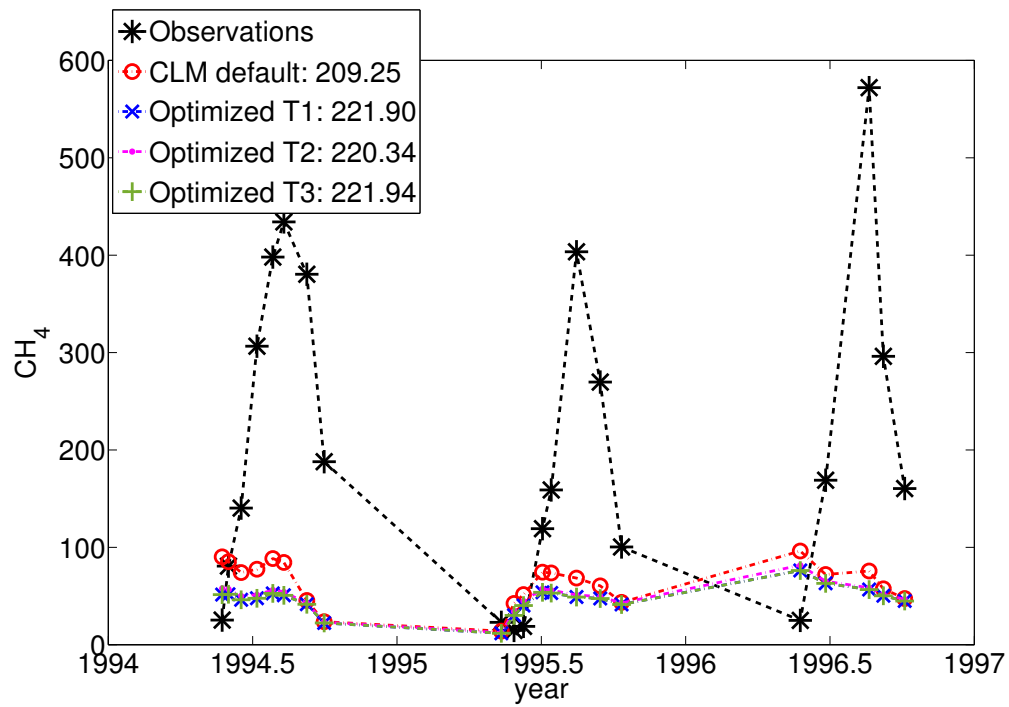


Figure 5. CH₄ emission observations and predictions when using the optimized parameters of optimization trials T1, T2, and T3, respectively, and when using the default parameters for the wetland site Alberta, Canada, for the real data case with $d = 5$ parameters. The legend shows the lowest RMSE value found in each trial.

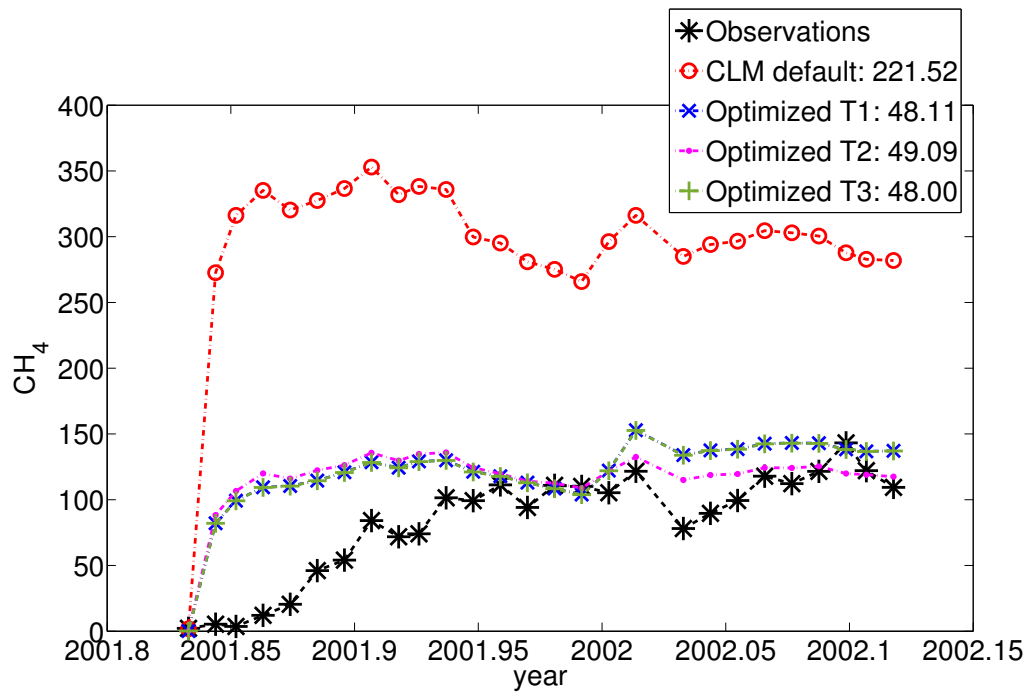


Figure 6. CH₄ emission observations and predictions when using the optimized parameters of optimization trials T1, T2, and T3, respectively, and when using the default parameters for the rice paddy site Central Java, Indonesia, for the real data case with $d = 5$ parameters. The legend shows the lowest RMSE value found in each trial.

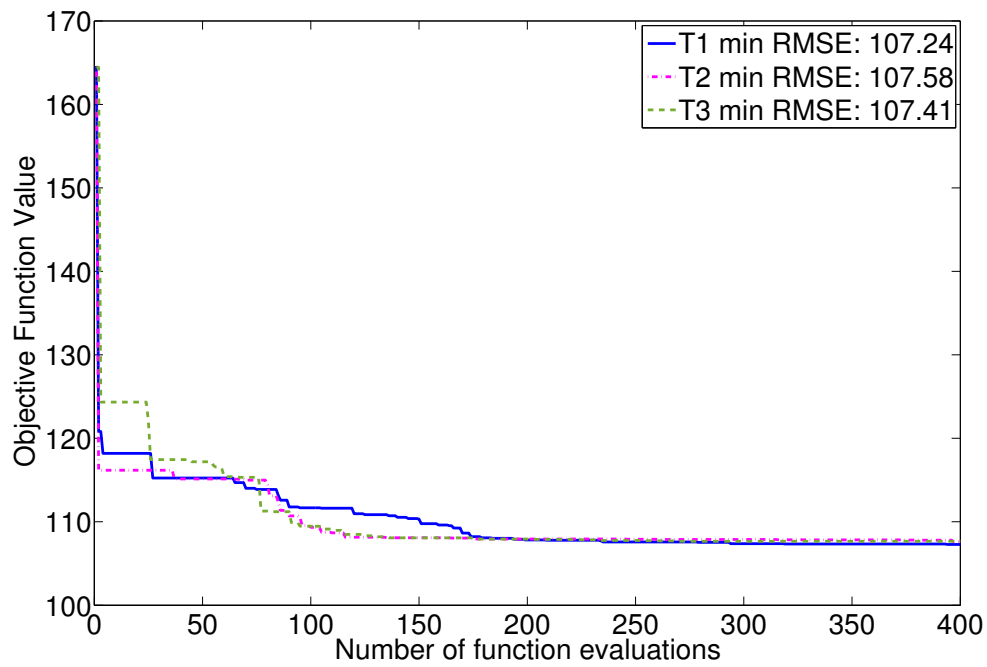


Figure 7. Progress plot that shows the development of the best objective function value found versus the number of function evaluations for the real data case with $d = 11$ parameters for optimization trials T1, T2, and T3. The legend shows the lowest RMSE value found in each trial. The first function evaluation (left side of the graphs) corresponds to the RMSE when using the default parameters.

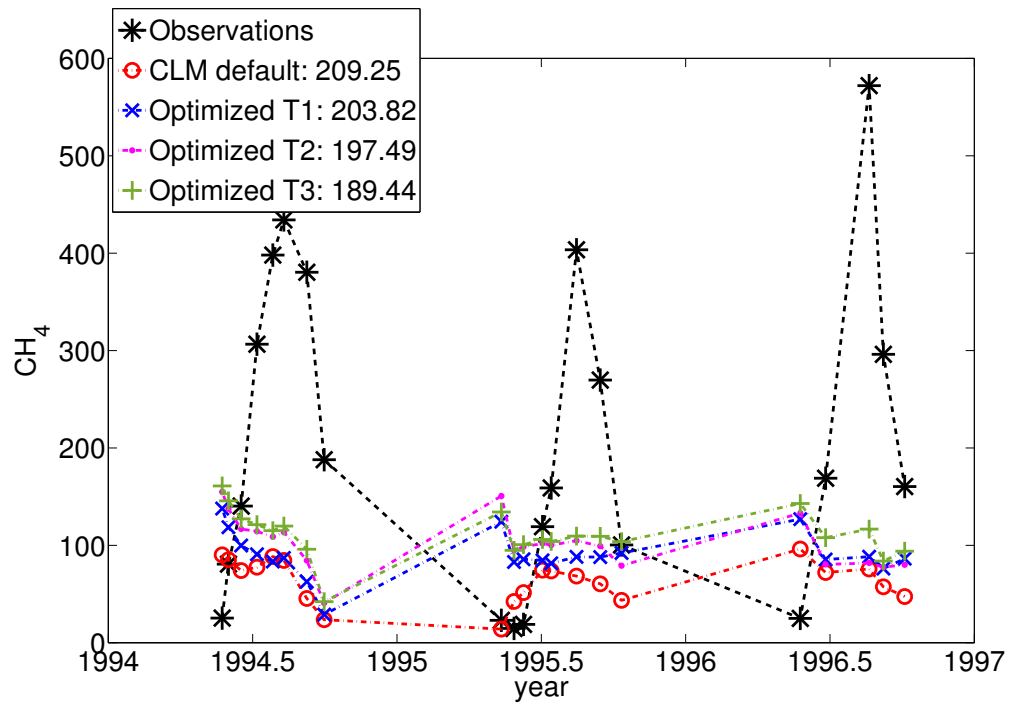


Figure 8. CH₄ emission observations and predictions when using the optimized parameters of optimization trials T1, T2, and T3, respectively, and when using the default parameters for the wetland site Alberta, Canada, for the real data case with $d = 11$ parameters. The legend shows the lowest RMSE value found in each trial.

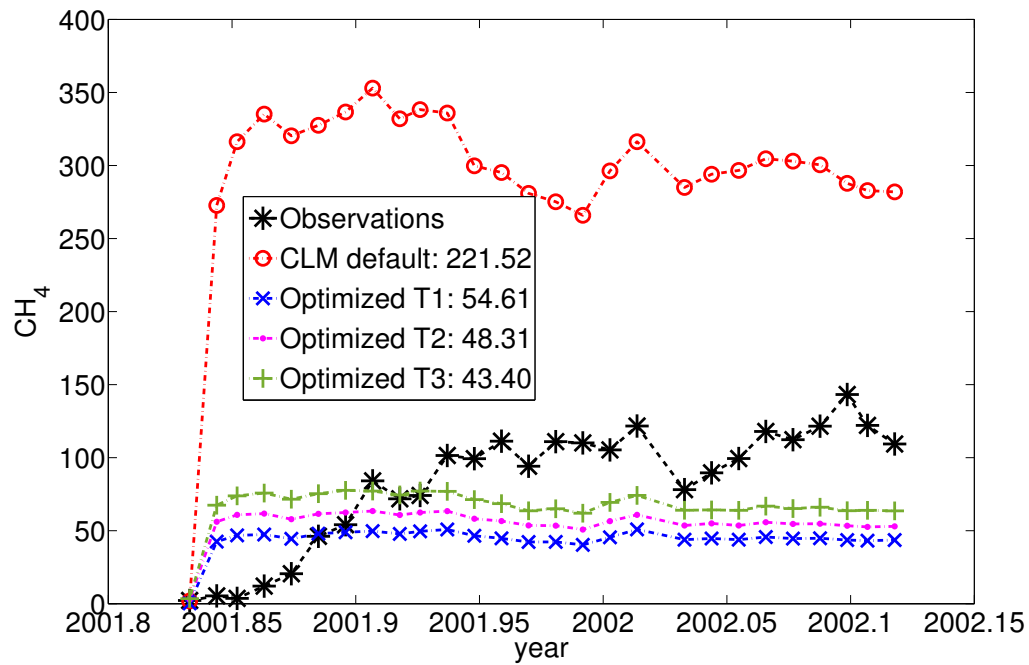


Figure 9. CH₄ emission observations and predictions when using the optimized parameters of optimization trials T1, T2, and T3, respectively, and when using the default parameters for the rice paddy site Central Java, Indonesia, for the real data case with $d = 11$ parameters. The legend shows the lowest RMSE value found in each trial.

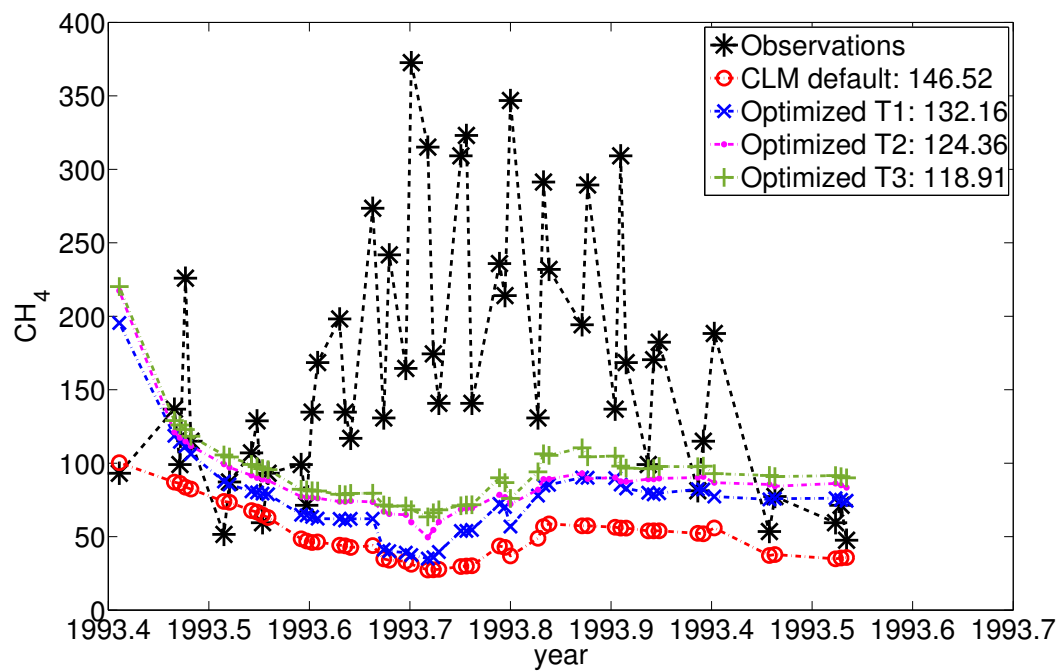


Figure 10. CH₄ emission observations and predictions when using the optimized parameters of optimization trials T1, T2, and T3, respectively, and when using the default parameters for the wetland site Salmisuo, Finland, for the real data case with $d = 11$ parameters. The legend shows the lowest RMSE value found in each trial.

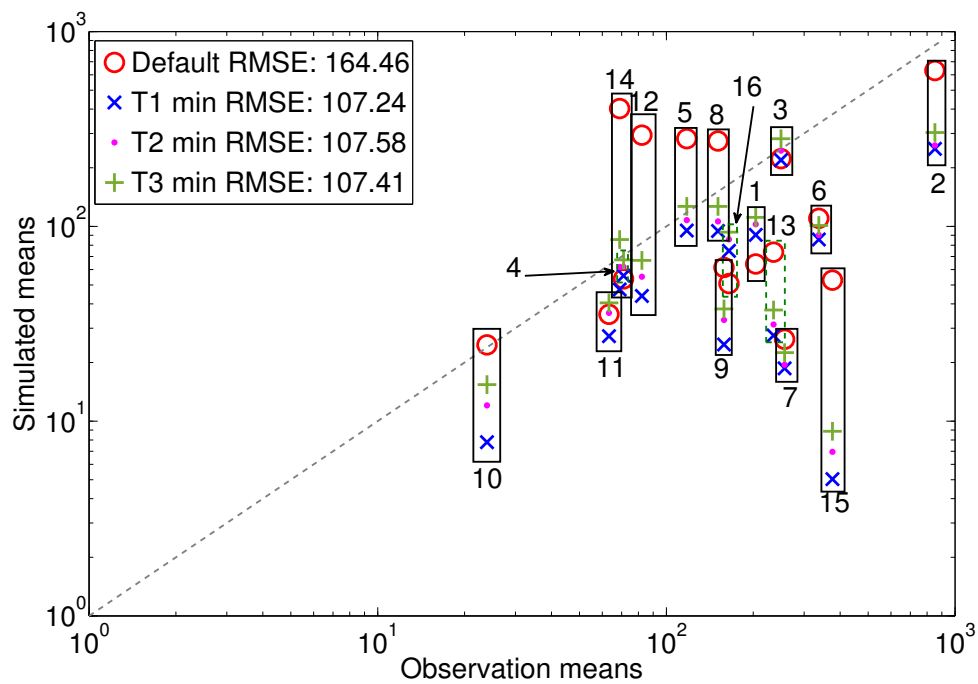


Figure 11. Scatterplot showing the mean values of the CH₄ predictions using the default and optimized parameter values of trials T1, T2, and T3, respectively, versus the mean values of the observations. The numbers in the legend show the best RMSE value corresponding to each trial. The numbers above/below the boxes indicate the observation site ID (1-Alberta, 2-Florida, 3-Michigan, 4-Minnesota, 5-Nanjing, 6-Vercelli, 7-Texas, 8-Japan, 9-California, 10-New Delhi, 11-Beijing, 12-Central Java, 13-Chengdu, 14-Cuttack, 15-Panama, 16-Salmisuo).

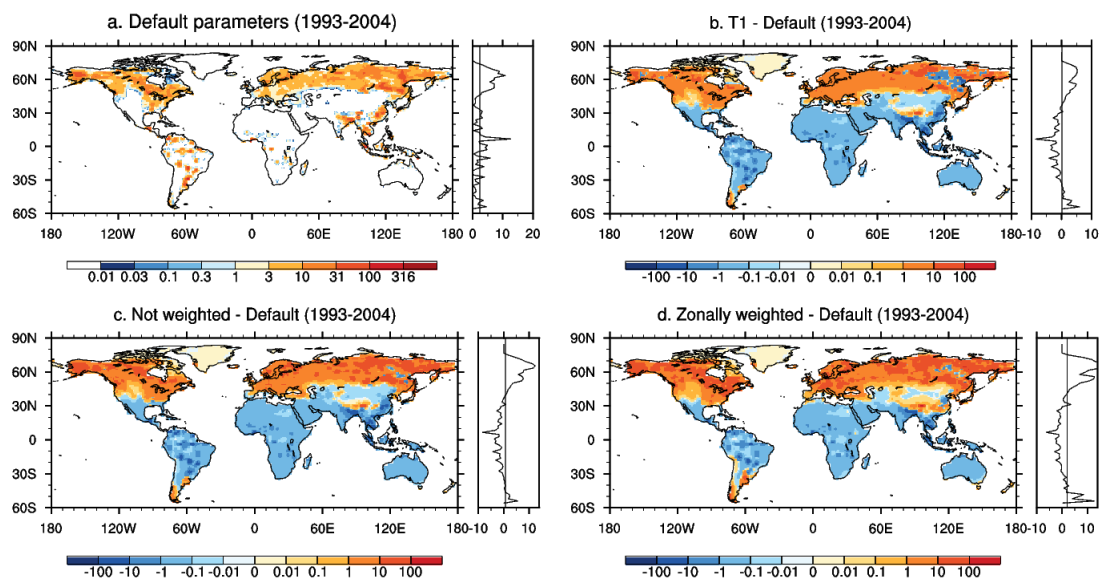


Figure 12. Average methane emissions ($\text{mg CH}_4\text{m}^{-2}\text{d}^{-1}$) simulated by CLM4.5bgc for (a) default parameters, (b) differences between default parameters and 11-dimensional optimization trial T1, (c) differences between default parameters and optimization trial with unweighted sum of RMSE, and (d) differences between default parameters and optimization trial with zonally weighted sum of RMSE. Zonal means are shown on the right side of each spatial plot.

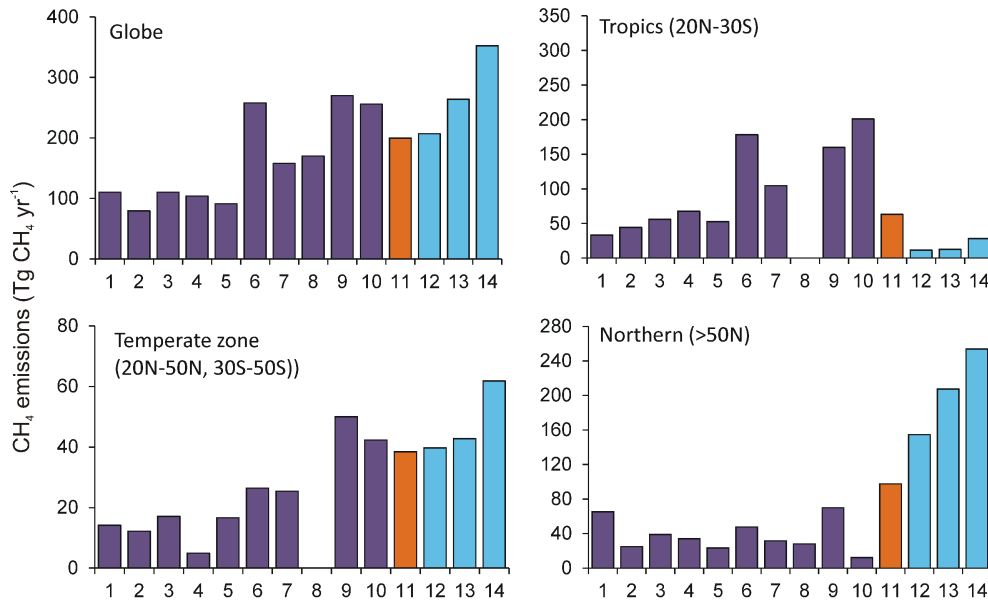


Figure 13. Comparison of total methane emissions ($\text{Tg CH}_4 \text{ yr}^{-1}$) between CLM4.5bgc and other models from natural wetlands. 1: Matthews and Fung (1987), 2: Aselmann and Crutzen (1989), 3: Bartlett et al. (1990), 4: Bartlett and Harriss (1993), 5: Cao et al. (1996), 6: Walter et al. (2001), 7: Bousquet et al. (2006), 8: Bloom et al. (2010), 9: CLM4Me, Riley et al. (2011), 10: CLM4Me', Meng et al. (2012), 11: This study, CLM4.5bgc with default parameters, 12: This study, CLM4.5bgc with $d = 11$ optimized parameters of T1, 13: This study, CLM4.5bgc with $d = 11$ optimized parameters of unweighted sum of RMSE, and 14: This study, CLM4.5bgc with $d = 11$ optimized parameters of zonally weighted RMSE. Note that number 7 is a top-down approach and number 9 may include the rice paddy emissions. For number 8, no data was available for the tropics and the temperate zone.